J. Fluid Mech. (1973), *vol.* 61, *part* 2, *pp.* 367–399
Printed in Great Britain

An experimental and numerical study of the viscous stability of a round laminar vertical jet with and without thermal buoyancy for symmetric and asymmetric disturbances

By J. C. MOLLENDORF
Engineering Research Center, Western Electric Co., Inc., Princeton, New Jersey
AND B. GEBHART
Upson Hall, Cornell University, Ithaca, New York

(Received 21 April 1972 and in revised form 1 March 1973)

The fully viscous hydrodynamic stability equations for a round laminar vertical jet have been numerically solved using the proper boundary-layer base-flow velocity profile and for both symmetric and asymmetric disturbances. The symmetric mode is found to be unconditionally stable. The first asymmetric mode is found to be unstable and characteristics are compared with previous calculations. The computed critical Reynolds number for this mode is 9·4, which agrees with the calculations of Burridge (1968). Disturbance amplitude-ratio contours are also calculated and related to the convection of disturbances in the flow.

The effect of thermal buoyancy on jet stability is assessed by solving the fully viscous equations, coupled through buoyancy, and using a buoyancy-perturbed jet flow. A Prandtl number σ of 6·7 is used, and positive thermal buoyancy is found to have a destabilizing effect. Stability characteristics for the limiting case of buoyancy, a purely thermal point-source plume, are determined for a Prandtl number of 2.

Finally, an experiment was performed using water jets in water ($\sigma \approx 4{\cdot}52$–$5{\cdot}89$) and a new method of jet production is described. The effect of varying amounts of thermal buoyancy on the laminar length of a jet undergoing naturally occurring transition was determined experimentally. These experiments confirm the calculated destabilizing effect of buoyancy. An empirical correlation is presented for the laminar length of a jet. Also, the effect of both symmetric and asymmetric artificially induced disturbances was determined experimentally. The disturbance amplitude ratio at which transition to turbulence takes place is found to be much less than for buoyant flows adjacent to a wall. The effects of frequency and amplitude of the artificial disturbances were experimentally determined and the trends are found to be consistent with the results of small disturbance theory.

The principal new result is that positive thermal buoyancy destabilizes jet flow, and consequently calls into question earlier experimental studies wherein

jet flows were observed by density differences. Another new result is the calculation of amplitude-ratio contours for a non-buoyant jet and the quantitative description of jet stability in terms of these contours along paths of constant physical frequency. A comparison of the non-buoyant theory with experimental jets containing varying amounts of thermal buoyancy indicates that transition did not occur at a well-defined value of the amplitude ratio. Perhaps experiments with truly non-buoyant jets and/or more detailed buoyant calculations could explain this remaining question.

1. Introduction

Jet stability and transition are important questions. Because of the large difference between laminar and turbulent transport characteristics, it is of great practical importance to know the conditions when one might expect each of these flow regimes. In technological processes one may wish to preserve the laminar nature of a jet for control purposes, or to induce turbulence for more vigorous transport. In addition, knowledge of the transition process may lead to the understanding of the mechanisms of related phenomena in some of the environmental flow configurations of recently increased importance.

Schlichting (1933) first calculated the velocity field for a round laminar jet using boundary-layer approximations. Landau (1943; see Landau & Lifshitz 1959) presented a solution which did not rely on these approximations. Neither analysis considered thermal diffusion. A solution for the uncoupled temperature field was given by Squire (1951) in a treatment nearly identical to that of Landau.

The effects of small amounts of thermal buoyancy in round laminar vertical jets has been investigated by Mollendorf & Gebhart (1973). The predominant effect of thermal buoyancy was found to be a change in the axial velocity component and a thinning of the jet. These calculated effects of buoyancy are used in the coupled part of the present stability analysis.

The stability, vortex-ring formation and transition to turbulence of Pfeifenton (pipe tone) jets was studied by Anderson (1954, 1955, 1956). The experimental set-up used was a $\frac{1}{4}$ in. orifice discharging CO_2 gas into air. A shadow graph was used to observe the flow and many beautiful pictures were presented. He determined the dependence of frequency on Reynolds number over a range of Re_D from 0 to 7000. The Reynolds number Re_D was calculated from physical conditions at the nozzle exit and the observed frequencies ranged from 880 to 6370 Hz. Although these jets were buoyant, no attempt was made to assess the effect of buoyancy on jet stability.

The first data known to us concerning the Reynolds number at which an axisymmetric jet becomes unstable were taken by Schade in 1958. The work is apparently unpublished, but the results are mentioned by Batchelor & Gill (1962). Schade apparently found that steady, laminar liquid-into-liquid jets could be obtained up to Reynolds numbers Re_D of several hundred. No definite critical Reynolds number was found. An experimental determination of the minimum Reynolds number for instability in a round jet was reported by Viilu (1962). Very small diameter (0·0052–0·018 in.) water-into-water jets were

observed using a 'sodium hydroxide, phenolthalene, hydrochloric acid' visualization technique. The Reynolds number Re_D for instability was found to be between 10·5 and 11·8. The discrepancy between the data of Schade and Viilu led Reynolds (1962) to investigate this problem further. Small diameter (0·0126 in.) dyed water jets were driven by a constant-head device into clear water. The velocity was calculated by measuring the mass flow rate of water emitted by the jet. The results indicated four modes of flow and instability, defined by ranges of the Reynolds number Re_D. For $10 < Re_D < 30$ it was difficult to maintain a long steady jet. For $30 < Re_D < 150$ the jets were longer. For $150 < Re_D < 300$ still longer jets were possible, but complex breakdown occurred. For $Re_D > 300$ the flow was predominately disordered even near the nozzle. In addition, spontaneous symmetric patterns were seen well away from the nozzle. These were called 'condensations'. Apparently, under certain conditions the condensations passed through one another in the manner of smoke rings.

Although there have been many studies concerning the stability of plane jets, the first analytical treatment of the axisymmetric ones was given by Batchelor & Gill. Linear, small disturbance theory was used with postulated disturbance amplitude growth, neutrality or attenuation with time. The analysis allowed for azimuthal [θ in figure 1 and in equations (7)–(11)] variations in the disturbance amplitude by including an azimuthal wavenumber n ($= 0, 1, 2, \ldots$). The case $n = 0$ can be thought of as a periodic local symmetric pulsing of the jet. For $n = 1$ there is a $\cos\theta$ variation in the disturbance magnitude. This is the first asymmetric mode. The flow appears to slosh locally but the disturbance to the motion amounts to a twisting fluted shape which moves downstream. It is like a turning screw which may slip (in x). Higher values of n result in more fluting.

Batchelor & Gill proved the existence of amplified disturbances for any value of the azimuthal wavenumber n for a 'top-hat', i.e. uniform, velocity profile. For Schlichting's velocity distribution, amplifying disturbances were found only for $n = 1$. They also solved the inviscid Orr–Sommerfeld equation for the 'top-hat' profile. The eigenfunctions are given by a linear combination of modified Bessel functions of the first and second kind, and the flow is unstable to small disturbances for all values of n and the axial wavenumber α. For Schlichting's profile (with a normalization different from that used here) and $n = 1$ the non-dimensional wavenumber α for neutral inviscid disturbances was found to be 1·46. This should perhaps be the limit at large Reynolds number for the upper branch of a neutral curve calculated including viscous effects.

The apparent contradiction between the observation of symmetric disturbances by Reynolds and the theory of Batchelor & Gill (i.e. the prediction of analysis that the flow is not unstable to symmetric disturbances) was investigated by Gill (1962). Gill's analysis indicated that symmetric disturbances do not grow in a slightly viscous fluid, but suggested that the growth of small but finite disturbances may be responsible for the condensations observed by Reynolds. A solution was given for disturbances of finite amplitude. Gill suggested that the agreement of his results with Reynolds' observations is due to the presence of appreciable background disturbances in the experimental apparatus of Reynolds.

Motivated by chemical reactor design considerations, McNaughton & Sinclair (1966) studied the flow of water through cylindrical vessels with an axial inlet and outlet, using a methylene blue dye-tracer. The inlet Reynolds number Re_D ranged from 100 to 28 000. In the lower range of Reynolds numbers they observed the same modes of breakdown as Reynolds. In addition, they presented an empirical relationship for the laminar length of a subturbulent jet as a function of the inlet Reynolds number, the diameter of the jet and the length and diameter of the flow vessel. It is interesting that they also stated that a small difference between the densities of the jet fluid and that in the vessel considerably affects the behaviour of the jet. They found that buoyancy thinned the jet in accordance with our results.

Becker & Massaro (1968) used air jets from a $\frac{1}{4}$ in. diameter nozzle and covered a Reynolds number range $Re_D = 600$–$20\,000$. Eight regimes of breakdown were suggested. By employing smoke photography, stroboscopic observation and a light-scatter technique (using both general illumination and sheet illumination through a slit) they correlated (with Reynolds number) such things as the formation of vortex rings, the coalescence of ring vortex pairs and the eventual disintegration into turbulent eddies. They investigated acoustic excitation and also discussed the effects of different nozzle configurations.

In an attempt to understand better the mechanisms of air pollution by chimney dispersal, Vignes (1968) studied vertical gaseous jets. She measured the maximum height attained by jets for several different heavier-than-air effluents. Nozzle diameters of 1·18 in. and less were used with flow conditions at Froude numbers of 150 and less. Her work deals with laminar jets and the density differences were larger than those of previous investigators. The jets were observed optically and their maximum height was measured with a hot-wire-grid device. It was shown that the maximum height is proportional to the Froude number for laminar jets and for jets experiencing transition. The constant of proportionality was found to depend on the gas used. The effect of the shape of the nozzle was also investigated. The penetration height was significantly higher for converging than for diverging nozzles, but was relatively insensitive to the angle of convergence or divergence.

Kambe (1969) reported the third† analysis concerning the stability of round jets. By assuming a parabolic axial velocity distribution in the jet, with a slope discontinuity around the edge, he was able to find analytical solutions of the uncoupled linearized stability equations for the disturbance forms $n = 0$, 1 and 2. He used the procedure of Batchelor & Gill for the 'top-hat' profile and postulated the same disturbance forms. Results for $n = 1$ and 2 were given as plots of the dimensionless wavenumber α *vs.* αR, where R is a momentum-flux parameter for various values of the complex wave speed. Both inviscid and viscous flow were analysed. For a symmetric disturbance ($n = 0$) the flow was found to be stable. For the inviscid case and $n \neq 0$ he suggested (after a partial investigation) that the flow is unstable for all non-zero n. Finally, for viscous flow and $n \neq 0$ the

† The review of the present work revealed a study by D. M. Burridge, at Bristol, who calculated the critical Reynolds number to be 9·4 for a non-buoyant jet in 1968.

critical Reynolds numbers were calculated to be $R_K = 32{\cdot}8$ and 171 for $n = 1$ and $n = 2$, respectively (R_K is the Reynolds number used in this study). The assumed flow is not related to a physical circumstance. However, if the profile satisfies a momentum-flux condition, then $R_K = R_B = 4R$, where R_B is the Reynolds number Batchelor & Gill used and R is the momentum-flux parameter to be used later here. Although the assumed parabolic velocity distribution is a good representation of the boundary-layer distribution near the axis of symmetry, it fails further out. In addition, it has the discontinuity noted above. Inflexion points are known to be very important in instability modes in other flows. This discontinuity may be very important.

Motivated by design considerations in fluidic devices (such as turbulence amplifiers), Marsters (1969) studied transition of small free jets. Carbon dioxide jets issuing from small (0·035–0·087 in.) nozzles into room temperature air were observed using a double-pass schlieren system. The principal result of this study is an empirical formula for the length L at which a laminar jet undergoes transition to turbulence, the so-called laminar length. A curve of the form $L/D = A Re_D^B$ provided a good correlation. Note that $Re_D \equiv V_j D/\nu$, where D is the diameter of the jet at the nozzle exit and V_j and ν are the jet velocity and viscosity at the nozzle exit. The values of A and B were 10^8 and $-2{\cdot}30$, respectively, for $Re_D < 2300$. A buoyancy effect parameter $Gr_{D,\Delta\rho}/Re_D^2$ was calculated to be 2×10^{-4}, where $Gr_{D\ \Delta\rho} \equiv gD^3(\rho_j - \rho_\infty)/\rho_j \nu^2$, and it was concluded that buoyant effects were small for the conditions of the experiments.

Another experimental investigation of laminar length was reported by McKenzie & Wall (1968). They also studied the effect of the interaction of two jets on laminar length for various conditions. However, their results for the undisturbed laminar length for a single jet differ considerably from those of Marsters. The constants A and B were found to be 10^3 and -1 for the low range of Reynolds numbers and L/D at which they observed transition. These two results are seen in figure 10. This latter work lacks adequate documentation but it appears that the jets studied may have been subject to large buoyancy effects. This question is discussed later in the light of our own experimental results.

In a detailed study by Crow & Champagne (1971), controlled disturbances were introduced at the nozzle exit of a free turbulent jet. They found that maximum amplification occurred at an imposed disturbance Strouhal number of 0·30. They also observed that the naturally occurring transition from sinous to pulsatile instability (at lower Reynolds numbers) was smooth and more continuous than that reported by Reynolds. They explain this difference by suggesting that the Reynolds vertical dye jet may have been slightly buoyant.

This summary of past work indicates that two different points of view have arisen in considering the stability and transition to turbulence of laminar jets. One (Marsters 1969) asks the question: at what distance downstream does a laminar jet undergo transition to turbulence? The other, linear stability theory (Batchelor & Gill 1962; Kambe 1969), postulates a small disturbance and asks the question: does it grow, attenuate or remain unaffected in its interaction with the jet?

The 'laminar-length' picture presupposes that the jet will become unstable

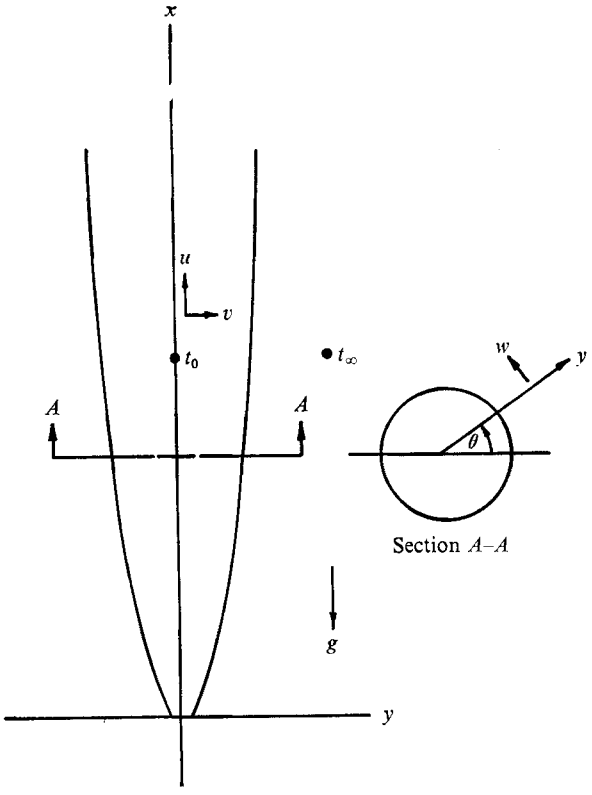

FIGURE 1. Cylindrical co-ordinate system for an axisymmetric jet.

somewhere downstream. Therefore, it concerns only jets which undergo transition before they effectively die out because of outward momentum diffusion. Stability-theory treatment also deals with jets which may be completely stable. We shall see later that our extensive stability-theory results, interpreted as a spacewise (x) amplitude growth, are consistent with the interpretation of jet transition in terms of laminar jet length. This provides the bridge between the two points of view.

The above summary indicates the principal things known about the stability and transition of axisymmetric laminar jets. The full viscous stability equations have apparently not been extensively treated for the velocity profile calculated by Schlichting. Furthermore, there has been no attempt to assess the effects of thermal buoyancy on stability, either in analysis or in experiment. Extensive previous study of two-dimensional natural convection flows adjacent to vertical and horizontal surfaces and in plumes has shown that 'buoyancy coupling' often has a very large effect on stability.

This study of round jets determines non-buoyant stability, including viscous effects and the use of the boundary-layer solution for the base flow. Then the effects of thermal buoyancy on stability are considered. This analysis uses our previous results (Mollendorf & Gebhart 1973) concerning the effect of a small amount of thermal buoyancy on the jet flow.

We first present the general coupled conservation equations. Disturbance equations are generated, disturbance forms are assumed and the appropriate boundary conditions are determined. Then numerical solutions are given for both the coupled and uncoupled full Orr–Sommerfeld equations for symmetric ($n = 0$) and for the more important asymmetric ($n = 1$) forms of disturbances.

Since the non-dimensional velocity and temperature base-flow profiles are identical for the non-buoyant jet and the axisymmetric thermal plume (for a Prandtl number of two), hydrodynamic stability results are presented for a purely buoyant axisymmetric plume subject to asymmetric ($n = 1$) disturbances for this Prandtl number. The governing equations are discussed in appendix A and the resulting neutral curve is shown on figure 8 with the various jet results. Plume stability results for other Prandtl numbers will appear in the future.

Finally, an experimental programme is described and comparison is made between experimentally measured and analytically predicted jet stability characteristics.

2. Analysis

2.1. *The stability equations*

The equations expressing the conservation of mass, momentum and energy are written in the cylindrical form most convenient for the flows considered here, as shown in figure 1. The Boussinesq approximation is incorporated and constant viscosity ν and thermal diffusivity α are assumed. Energy effects associated with viscous dissipation and, for example, the pressure term $\beta T Dp/D\tau$, are neglected. The equations, in terms of instantaneous-flow quantities, are

$$\frac{\partial}{\partial x}(yu)+\frac{\partial}{\partial y}(yv)+\frac{\partial w}{\partial \theta}=0, \tag{1}$$

$$\frac{\partial u}{\partial \tau}+u\frac{\partial u}{\partial x}+v\frac{\partial u}{\partial y}+\frac{w}{y}\frac{\partial u}{\partial \theta}+\frac{1}{\rho}\frac{\partial p}{\partial x}=\nu\nabla^2 u-g, \tag{2}$$

$$\frac{\partial v}{\partial \tau}+u\frac{\partial v}{\partial x}+v\frac{\partial v}{\partial y}+\frac{w}{y}\frac{\partial v}{\partial \theta}-\frac{w^2}{y}+\frac{1}{\rho}\frac{\partial p}{\partial y}=\nu\left(\nabla^2 v-\frac{v}{y^2}-\frac{2}{y^2}\frac{\partial w}{\partial \theta}\right), \tag{3}$$

$$\frac{\partial w}{\partial \tau}+u\frac{\partial w}{\partial x}+v\frac{\partial w}{\partial y}+\frac{w}{y}\frac{\partial w}{\partial \theta}+\frac{vw}{y}+\frac{1}{\rho y}\frac{\partial p}{\partial \theta}=\nu\left(\nabla^2 w+\frac{2}{y^2}\frac{\partial v}{\partial \theta}-\frac{w}{y^2}\right), \tag{4}$$

$$\frac{\partial t}{\partial \tau}+u\frac{\partial t}{\partial x}+v\frac{\partial t}{\partial y}+\frac{w}{y}\frac{\partial t}{\partial \theta}=\alpha\nabla^2 t, \tag{5}$$

$$\nabla^2\equiv\frac{\partial^2}{\partial y^2}+\frac{1}{y}\frac{\partial}{\partial y}+\frac{1}{y^2}\frac{\partial^2}{\partial \theta^2}+\frac{\partial^2}{\partial x^2}, \tag{6}$$

where τ is time and t temperature.

The stability analysis of a boundary-layer flow proceeds by perturbing the steady laminar flow $\{U_0, V_0, \text{etc.}\}$, called the base flow, with postulated disturbances $\{u', v', \text{etc.}\}$. Linear theory follows by neglecting nonlinear terms in the disturbance magnitudes, justifiable for small disturbance amplitude. The disturbances are assumed periodic and one may specify exponential damping or

amplification with either downstream distance x or time τ. Amplification with downstream distance is more closely related to actual flow and lends itself to comparison with experimental data. For this reason distance amplification will be postulated here. Batchelor & Gill formulated the equations in terms of time amplification of disturbances and Kambe followed the same procedure. Only periodic behaviour of disturbance quantities is admitted in the azimuthal direction θ. The disturbance quantities are postulated as

$$u'(x,y,\theta,\tau) = \mathrm{Re}\{\hat{F}(y)\exp[i(\hat{\alpha}x-\hat{\beta}\tau+n\theta)]\}, \tag{7}$$

$$v'(x,y,\theta,\tau) = \mathrm{Re}\{\hat{G}(y)\exp[i(\hat{\alpha}x-\hat{\beta}\tau+n\theta)]\}, \tag{8}$$

$$w'(x,y,\theta,\tau) = \mathrm{Re}\{\hat{H}(y)\exp[i(\hat{\alpha}x-\hat{\beta}\tau+n\theta)]\}, \tag{9}$$

$$p'(x,y,\theta,\tau) = \mathrm{Re}\{\hat{I}(y)\exp[i(\hat{\alpha}x-\hat{\beta}\tau+n\theta)]\}, \tag{10}$$

$$t'(x,y,\theta,\tau) = \mathrm{Re}\{\hat{J}(y)\exp[i(\hat{\alpha}x-\hat{\beta}\tau+n\theta)]\}, \tag{11}$$

where $\hat{F}$, $\hat{G}$, $\hat{H}$, $\hat{I}$ and $\hat{J}$ are the complex dimensional amplitude functions and $\hat{\alpha}$ is complex. The real part of $\hat{\alpha}$ is the dimensional wavenumber $2\pi/\lambda$ in the x direction, where λ is the physical wavelength. The imaginary part is the exponential amplification rate in the x direction. Hence, the amplitude of the disturbance increases with x for $\alpha_i < 0$, attenuates for $\alpha_i > 0$ and is neutral for $\alpha_i = 0$. The quantity $\hat{\beta}$ is taken to be real and equal to $2\pi f$, where f is the physical frequency of the disturbance. The azimuthal wavenumber n characterizes the θ dependence of the disturbance quantities and has integer values, say the positive ones, i.e. $n = 0, 1, 2, 3, \ldots$. The value of n determines much of the spatial character of the disturbance as will be discussed in the next section.

We shall simultaneously consider both jet and plume flows. The characteristic length L_c, velocity V_c and temperature T_c for jet flow are

$$L_c = x/R, \tag{12}$$

$$V_c = \nu R^2/x, \tag{13}$$

$$T_c = t_0 - t_\infty \equiv \Delta t_0 \propto 1/x, \tag{14}$$

where R is the 'momentum-flux parameter' defined by Mollendorf & Gebhart as $R \equiv (3M/16\pi\mu\nu)^{\frac{1}{2}}$, where M is the momentum flux across a plane normal to the axis of the jet and μ and ν are the viscosities. The actual nozzle Reynolds number is a function of the velocity distribution at the nozzle. For a parabolic velocity distribution $Re_D = 4R$ and for a top-hat velocity distribution $Re_D = (8/\sqrt{3})R$. The characteristic quantities for an axisymmetric plume are the same when R is $(\frac{1}{4}Gr_{x,\Delta t_0})^{\frac{1}{4}}$ (see appendix A). The base flow and time-dependent disturbances, when scaled with these characteristic quantities, are written without the caret, e.g. $\hat{F}/V_c \equiv F$.

The instantaneous-flow quantities, e.g. $u = U_0 + u'$, are substituted into (1)–(6). The results are linearized in disturbance quantities and boundary-layer approximations are applied to the base flow. Several additional approximations are required concerning α and several non-parallel terms. These are justifiable when the thickness of the flow region changes sufficiently slowly downstream.

The disturbance equations, in terms of the disturbance amplitude distributions F, G, H, I and J, are

$$\alpha\eta F - i(\eta G)' + nH = 0, \tag{15}$$

$$i\alpha(U_0 - \beta/\alpha)F + GU_0' = \frac{1}{R}\left[F'' + \frac{1}{\eta}F' - \left(\alpha^2 + \frac{n^2}{\eta^2}\right)F\right] - i\alpha I + \frac{\epsilon}{R}J, \tag{16}$$

$$i\alpha(U_0 - \beta/\alpha)G = \frac{1}{R}\left[G'' + \frac{1}{\eta}G' - \left(\alpha^2 + \frac{n^2+1}{\eta^2}\right)G - \frac{2in}{\eta^2}H\right] - I', \tag{17}$$

$$i\alpha(U_0 - \beta/\alpha)H = \frac{1}{R}\left[H'' + \frac{1}{\eta}H' - \left(\alpha^2 + \frac{n^2+1}{\eta^2}\right)H + \frac{2in}{\eta^2}G\right] - \frac{in}{\eta}I, \tag{18}$$

$$i\alpha(U_0 - \beta/\alpha)J + GT_0' = \frac{1}{\sigma R}\left[J'' + \frac{1}{\eta}J' - \left(\alpha^2 + \frac{n^2}{\eta^2}\right)J\right]. \tag{19}$$

The primes above indicate differentiation with respect to the independent similarity variable $\eta = Ry/x$. The Prandtl number is $\sigma = \nu/\alpha$ and for a non-buoyant jet, $U_0 = 2(1+\frac{1}{4}\eta^2)^{-2}$ and $T_0 = (1+\frac{1}{4}\eta^2)^{-2\sigma}$. Equations (15)–(19) may be shown to be identical to those of Batchelor & Gill by substituting iG for G above and taking $\epsilon = 0$. Note that $\epsilon(x)$ in (16) above is the buoyancy perturbation parameter defined in Mollendorf & Gebhart as $\epsilon(x) = Gr/R^4$, where

$$Gr \equiv g\beta x^3 \Delta t_0/\nu^2.$$

The predominant effect of positive thermal buoyancy is to increase the axial velocity component of the jet base flow in the region of the thermal boundary layer and to reduce it slightly at larger y. The magnitude of the effect increases as the Prandtl number decreases. For a Prandtl number of 6·7 the increase in the axial velocity component is about 7 % near the jet axis. For non-zero values of ϵ the disturbance energy equation in J is coupled to the others through the buoyancy body-force term. The above set of five equations for the five unknown eigenfunctions F, G, H, I and J, along with the appropriate boundary conditions, constitutes an eigenvalue problem whose solution predicts the stability characteristics of the prescribed base flow. Boundary conditions are considered below.

2.2. *Disturbance boundary conditions*

The proper set of boundary conditions for (15)–(19) depends on the value of the azimuthal wavenumber n to be used. From (7)–(11) the various dimensionless disturbance quantities are given as follows:

$$u'(x, y, \theta, \tau) = |F|\, e^{-\alpha_i x} \cos(\alpha_r x - \beta\tau + n\theta + \theta_F), \tag{20}$$

$$v'(x, y, \theta, \tau) = |G|\, e^{-\alpha_i x} \cos(\alpha_r x - \beta\tau + n\theta + \theta_G), \tag{21}$$

$$w'(x, y, \theta, \tau) = |H|\, e^{-\alpha_i x} \cos(\alpha_r x - \beta\tau + n\theta + \theta_H), \tag{22}$$

$$p'(x, y, \theta, \tau) = |I|\, e^{-\alpha_i x} \cos(\alpha_r x - \beta\tau + n\theta + \theta_I), \tag{23}$$

$$t'(x, y, \theta, \tau) = |J|\, e^{-\alpha_i x} \cos(\alpha_r x - \beta\tau + n\theta + \theta_J). \tag{24}$$

Note that $|F|$, $|G|$, etc., are the magnitudes of complex numbers, e.g.

$$|F|^2 \equiv \mathrm{Re}^2\{F\} + \mathrm{Im}^2\{F\},$$

and θ_F, θ_G, etc., are phase angles, i.e.

$$\theta_F \equiv \tan^{-1}(\mathrm{Im}\{F\}/\mathrm{Re}\{F\}).$$

Since for any value of n the disturbance quantities must go to zero at large y, we have

$$u' = v' = w' = p' = t' = 0 \quad \text{as} \quad y \to \infty. \tag{25}$$

The proper boundary conditions on the jet axis depend on n. For $n = 0$, no θ variation, we have symmetry about the jet axis. Therefore w' is everywhere zero and the boundary conditions on the axis are

$$\frac{\partial u'}{\partial y} = v' = w' = \frac{\partial p'}{\partial y} = \frac{\partial t'}{\partial y} = 0 \quad \text{at} \quad y = 0. \tag{26}$$

For $n = 1$ there is a $\cos\theta$ variation in the disturbance quantities. This is the simplest asymmetric mechanism. Since the scalar quantities p' and t' cannot be multi-valued when approaching the axis radially at different values of θ, they must vanish on the axis of the jet. The same is true for u' since it is directed along the axis of the jet. However, the radial and azimuthal components v' and w' of the disturbance velocity lie in a plane perpendicular to the axis of the jet. It may be seen from the nature of the co-ordinate system that on the axis of the jet v' and w' are equal in magnitude but out of phase by ninety degrees. Further, non-zero values of v' and w' are possible only for $n = 1$.

In terms of the amplitude functions, the boundary conditions become

$$\left.\begin{aligned} F'(0) = G(0) = I'(0) = J'(0) = 0 \\ F(\infty) = G(\infty) = I(\infty) = J(\infty) = 0 \end{aligned}\right\} \quad \text{for} \quad n = 0, \tag{27}$$

$$\left.\begin{aligned} F(0) = I(0) = J(0) = G(0) + iH(0) = 0, \\ F(\infty) = G(\infty) = H(\infty) = I(\infty) = J(\infty) = 0, \end{aligned}\right\} \quad \text{for} \quad n = 1, \tag{28}$$

$$\left.\begin{aligned} F(0) = G(0) = H(0) = I(0) = J(0) = 0, \\ F(\infty) = G(\infty) = H(\infty) = I(\infty) = J(\infty) = 0. \end{aligned}\right\} \quad \text{for} \quad n \neq 0, 1. \tag{29}$$

The boundary conditions for a given n are not all necessarily independent. The required number is equal to the overall order of the system of differential equations. The asymptotic behaviour of the equations for both $n = 0$ and $n = 1$ is dealt with in the next subsection.

2.3. *Asymptotic behaviour of the stability equations*

Symmetric disturbances ($n = 0$). For symmetric disturbances (i.e. $\partial/\partial\theta = w' = 0$) equations (1)–(6) are much simpler. The continuity equation is satisfied by introducing a disturbance stream function

$$\hat{\psi}(x, y, \tau) = \hat{\phi}(y) \exp\{i(\hat{\alpha}x - \hat{\beta}\tau)\}, \tag{30}$$

such that

$$u' = \mathrm{Re}\left\{\frac{\nu}{y}\hat{\psi}_y\right\}, \quad v' = \mathrm{Re}\left\{-\frac{\nu}{y}\hat{\psi}_x\right\}. \tag{31), (32}$$

The pressure is eliminated by cross-differentiation and the dimensionless Orr–Sommerfeld equations in cylindrical co-ordinates are found to be

$$i\alpha R[(U_0-\beta/\alpha)D\phi-\eta(U_0'/\eta)'\phi] = D^2\phi+\epsilon\eta J', \tag{33}$$

$$i\alpha\sigma R\left[(U_0-\beta/\alpha)J-\frac{T_0'}{\eta}\phi\right] = J''+\frac{J'}{\eta}-\alpha^2 J, \tag{34}$$

where primes indicate differentiation with respect to η and the differential operator D is given by

$$D \equiv \frac{d^2}{d\eta^2}-\frac{1}{\eta}\frac{d}{d\eta}-\alpha^2. \tag{35}$$

The boundary conditions are written as

$$\left.\begin{aligned}(\phi'/\eta)' = \phi/\eta = J' = 0 \quad &\text{at} \quad \eta = 0,\\ \phi'/\eta = \phi/\eta = J \to 0 \quad &\text{as} \quad \eta\to\infty.\end{aligned}\right\} \tag{36}$$

The solution of (33) for large η and $\epsilon = 0$, satisfying (36), is

$$\begin{aligned}\phi \sim C_1\eta^{\frac{1}{2}}e^{-\gamma\eta}\left[1+\left(\frac{3}{8\gamma}\right)\eta^{-1}-\left(\frac{15}{128\gamma^2}\right)\eta^{-2}+\ldots\right]\\ +C_2\eta^{\frac{1}{2}}e^{-\alpha\eta}\left[1+\left(\frac{3}{8\alpha}\right)\eta^{-1}-\left(\frac{15}{128\alpha^2}\right)\eta^{-2}+\ldots\right],\end{aligned} \tag{37}$$

where C_1 and C_2 are arbitrary constants and $\gamma^2 \equiv \alpha^2 - i\beta R$. This is the expansion of a modified Bessel function of the second kind for large argument. The behaviour of ϕ for small argument is as follows:

$$\phi \sim C_3\eta^2[1+b_2\eta^2+b_4\eta^4+\ldots]+C_4\eta^2\left[1+\frac{\alpha^2}{8}\eta^2+\frac{\alpha^4}{192}\eta^4+\ldots\right], \tag{38}$$

where C_3 and C_4 are arbitrary constants and

$$b_2 \equiv \tfrac{1}{8}(\xi^2+\alpha^2) \quad \text{and} \quad b_4 \equiv \tfrac{1}{192}(\xi^4+\xi^2\alpha^2+\alpha^4),$$

where $\xi^2 \equiv \alpha^2+i\alpha R(2-\beta/\alpha)$.

Equations (37) and (38) will form the basis for the numerical solution of (33) for $\epsilon = 0$. For non-zero values of the perturbation parameter $\epsilon(x)$, equations (33) and (34) are coupled through the buoyancy-force term. A slightly different numerical technique is used to account for buoyancy coupling and only the expansion for small η is needed. It can be shown that coupling plays a rather small role in the expansions for small η and alters (38) by an additional term of $O(\eta^6)$. For the numerical technique to be used with coupling for $n = 0$ this alteration is not needed. Similarly, the expansion for the disturbance temperature function J is affected only in higher order terms by buoyancy coupling and is given by

$$J = C_5[1+\zeta^2\eta^2+\ldots], \tag{39}$$

where C_5 is an arbitrary constant and $\zeta^2 \equiv \alpha^2+i\alpha\sigma R(2-\beta/\alpha)$.

Asymmetric disturbances ($n = 1$). Just as symmetric disturbances ($n = 0$) could be simplified by using a stream function, the equations for the case $n = 1$

can be simplified by defining new variables. This was done in a rather general way by Kambe for any value of n. Kambe did not consider the disturbance energy equation, but it will be given here with the other results for $n = 1$. The technique consists of eliminating F and I in (15)–(19) and defining new variables and differential operators. The resulting equations (for $n = 1$) are

$$D_1\Delta_2^\alpha T - D_{-1}\Delta_0^\alpha S = i\alpha R\{(U_0-\beta/\alpha)(D_1T - D_{-1}S) + U_0'(T-S)\}, \tag{40}$$

$$E_1\Delta_2^\alpha T + E_{-1}\Delta_0^\alpha S = i\alpha R\{(U_0-\beta/\alpha)(E_1T + E_{-1}S) - U_0'(T+S)\} + 2\epsilon\alpha J, \tag{41}$$

$$\Delta_1^\alpha J = i\alpha\sigma R(U_0-\beta/\alpha)J + \tfrac{1}{2}i\sigma R(T+S)T_0', \tag{42}$$

where

$$S \equiv -iG - H, \quad T \equiv -iG + H \tag{43}$$

and

$$\Delta_m^\alpha \equiv \frac{d^2}{d\eta^2} + \frac{1}{\eta}\frac{d}{d\eta} - \frac{m^2}{\eta^2} - \alpha^2, \tag{44}$$

$$D_n \equiv \frac{d}{d\eta} + \frac{1+n}{\eta}, \quad E_n \equiv D_n + \frac{\alpha^2}{n}\eta. \tag{45), (46}$$

G and H are written in terms of the new variables S and T as

$$G = \tfrac{1}{2}i(T+S), \quad H = \tfrac{1}{2}(T-S). \tag{47}$$

The expansions for the amplitude functions on the axis of the jet for $n = 1$ are

$$F \sim C_1\eta + a_3\eta^3 + O(\eta^5), \tag{48}$$

$$G \sim C_5 + C_6\eta^2 + b_4\eta^4 + O(\eta^6), \tag{49}$$

$$H \sim iC_5 + (3iC_6 - \alpha C_1)\eta^2 + (5ib_4 - \alpha a_3)\eta^4 + O(\eta^6), \tag{50}$$

$$I \sim d_1\eta + d_2\eta^3 + O(\eta^5), \tag{51}$$

$$J \sim C_3\eta + O(\eta^3), \tag{52}$$

where a_3, b_4, d_1 and d_2 are rather cumbersome relations involving C_1, C_3, C_5 and C_6 and will not be written here since it is convenient to solve the governing equations numerically in terms of S and T (defined by (43)). By using (49) and (50) to determine the expansions for S and T we arrive at

$$S \sim A + B\eta^2 + C\eta^2 + O(\eta^4), \tag{53}$$

$$T \sim -\tfrac{1}{2}B\eta^2 - C\eta^2 + O(\eta^4), \tag{54}$$

$$J \sim D\eta + O(\eta^3), \tag{55}$$

where $A \equiv -2iC_5$, $B \equiv -4iC_6$, $C \equiv \alpha C_1$ and $D \equiv C_3$. The above expansions in terms of the four arbitrary constants A, B, C and D will form the basis for the numerical solution of (40)–(42).

2.4. *Numerical solution and results*

Symmetric disturbances ($n = 0$). The numerical scheme used to solve the fourth-order, two-point boundary-value, eigenvalue problem posed by (33) and (34), subject to the boundary conditions (36), relies on the linear nature of the equations and boundary conditions. Superposition is used in the numerical technique

described by Hieber & Gebhart (1971). The method used here for the case $n = 0$ and $\epsilon = 0$ is different in that expansions are used both as $\eta \to \infty$ and at $\eta = 0$ and the unknown constants are determined by 'patching' near the middle of the boundary layer, at η_p. Starting with the expansions (37), we take $C_1 \equiv 1$, without loss of generality, since the governing equations and boundary conditions are homogeneous and linear. Then particular real values are taken for R and β and a complex α is guessed. At large η ($\eta = \eta_e$, say) equation (37) is used to evaluate $\phi \sim C_1\phi + C_2\phi_2$ and the necessary derivatives needed to start the integration. Typically η_e is taken to be 10. A modified Hammings predictor–corrector is used to integrate the equations in to η_p and the values of ϕ_1 and its derivatives at η_p are stored. The same is done for ϕ_2.

Next the expansion at $\eta = 0$ (equation (38), i.e. $\phi \sim C_3\phi_3 + C_4\phi_4$) is used to provide the proper starting values, the integrations are performed from $\eta = 0$ to $\eta = \eta_p$ and the values of the functions at η_p are stored. The patching procedure consists of satisfying the following relations at $\eta = \eta_p$:

$$C_3\phi_3 + C_4\phi_4 = \phi_1 + C_2\phi_2, \tag{56}$$

$$C_3\phi_3' + C_4\phi_4' = \phi_1' + C_2\phi_2', \tag{57}$$

$$C_3\phi_3'' + C_4\phi_4'' = \phi_1'' + C_2\phi_2'', \tag{58}$$

$$C_3\phi_3''' + C_4\phi_4''' = \phi_1''' + C_2\phi_2'''. \tag{59}$$

When the above relations are satisfied, the fourth and all higher order derivatives will match since the governing equation is of fourth order. This system of four equations involves three unknown constants C_2, C_3 and C_4, and only three of the equations can be satisfied by solving for C_2, C_3 and C_4. The remaining relation is satisfied by the proper choice of the eigenvalue α. So if (57)–(59) are used to solve for C_2, C_3 and C_4 then (56) can be satisfied only by the proper choice of α. The correct value of α is determined iteratively as follows. Having determined C_2, C_3 and C_4 we define

$$f \equiv C_3\phi_3 + C_4\phi_4 - \phi_1 - C_2\phi_2. \tag{60}$$

We now seek an α such that $f(\eta_p) \equiv 0$. Let the correct value of α be denoted by α_0 and the first guess by α_1. We can expand about the initial guess in a Taylor series as follows:

$$f(\alpha_0) = 0 = f(\alpha_1) + \delta\alpha \frac{df(\alpha_1)}{d\alpha} + \dots. \tag{61}$$

By using only the first two terms of (61) we can solve for $\delta\alpha$ at $\alpha = \alpha_1$:

$$\delta\alpha = -f(\alpha) \Big/ \frac{df}{d\alpha}. \tag{62}$$

The derivatives with respect to α are obtained from the equations, boundary conditions and expansions and integrated along with the governing equations. The new guess for $\alpha = \alpha_2$ is then given by (62) as

$$\alpha_2 = \alpha_1 + \delta\alpha. \tag{63}$$

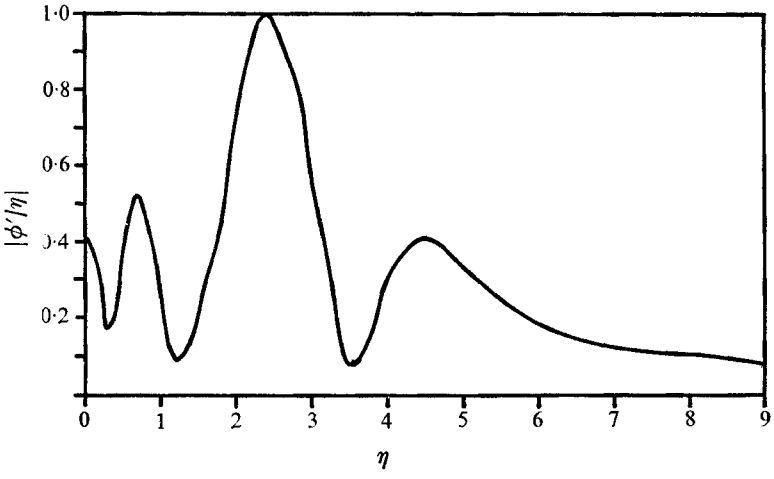

FIGURE 2. Typical highly damped eigenfunction for a non-buoyant jet ($\epsilon = 0$) and disturbance mode $n = 0$. $R = 20$, $\beta = 0{\cdot}20$, $\alpha_r = 0{\cdot}2863$, $\alpha_i = 0{\cdot}7956$.

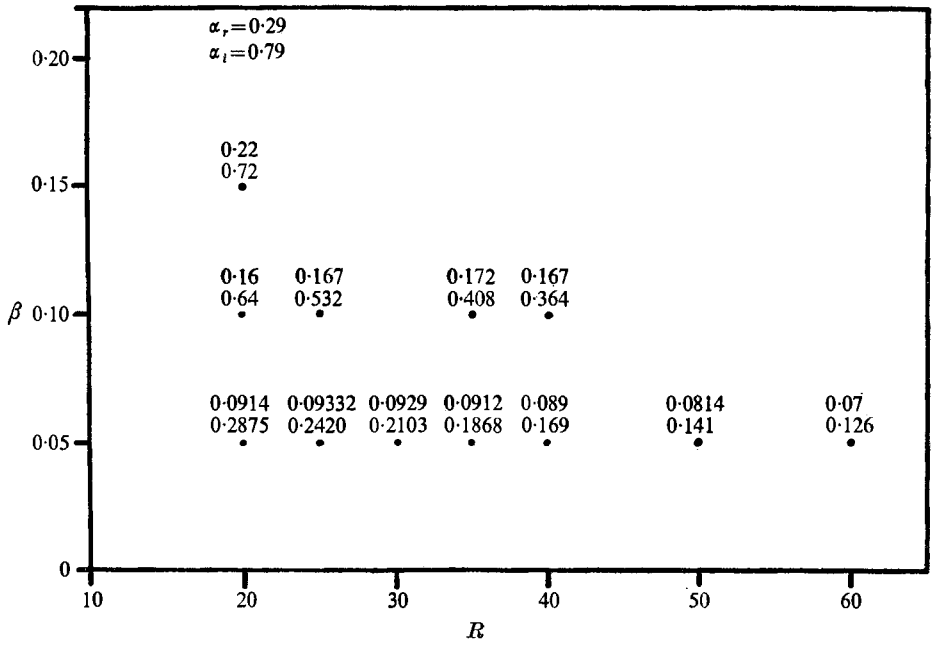

FIGURE 3. Eigenvalues for a non-buoyant jet ($\epsilon = 0$) and disturbance mode $n = 0$.

By successively iterating on α, it is possible to converge to a solution which satisfies the governing equations and boundary conditions for the specified β and R.

A typical eigenfunction is shown in figure 2 for a damped condition, $\alpha_i > 0$. It exhibits the same general shape and complexity as the damped eigenfunctions found by Knowles & Gebhart (1968) for natural convection adjacent to a vertical plate. Although the equations (for $n = \epsilon = 0$) were solved for many values of β

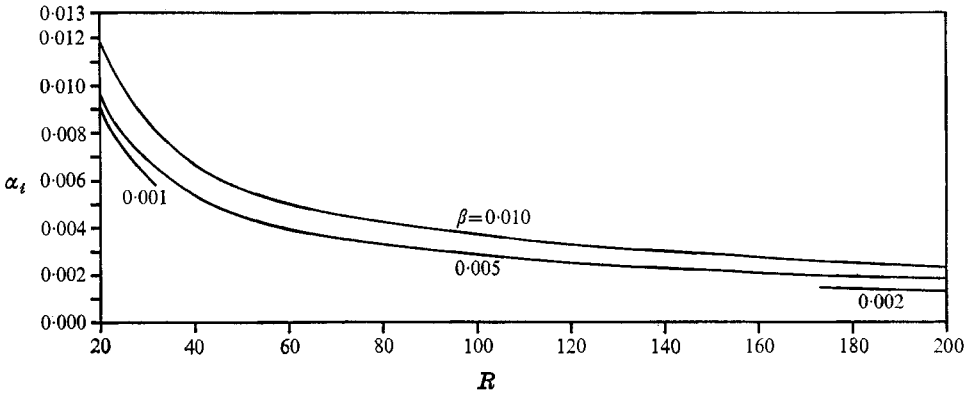

FIGURE 4. Behaviour of α_i *vs.* R for various values of β for the disturbance mode $n = 0$ and $\epsilon = 0$.

and R, none of the results yielded either neutrally stable points ($\alpha_i = 0$) or amplified ones ($\alpha_i < 0$). Some damped points are shown on figure 3 for $n = 0$. The absence of disturbance amplification for the mode $n = 0$ is in agreement with the analyses of Batchelor & Gill and of Kambe for the 'top-hat' and 'discontinuous-parabola' base-flow distributions, respectively. The α_i *vs.* R behaviour for fixed β as calculated for $n = \epsilon = 0$ is shown in figure 4. This figure suggests that α_i tends to zero very slowly for large values of R and small values of β.

The effect of buoyancy coupling was also explored for the symmetric mode $n = 0$, for $-1 \leqslant \epsilon \leqslant +1$. A slightly different numerical technique was used. As mentioned previously, the effect of buoyancy coupling was shown to have an effect only on higher order terms in the series expansions at $\eta = 0$. Therefore, it was convenient to integrate the full coupled equations from $\eta = 0$ to $\eta = \eta_e$ using the expansions at $\eta = 0$ to provide the starting values. This problem is a sixth-order, two-point boundary-value, eigenvalue problem. We must guess and then iterate on $\phi''(0)$, $J(0)$ and α, such that the disturbance velocities and temperature go to zero as $\eta \to \infty$. This procedure agreed with the aforementioned uncoupled patching technique for $\epsilon = 0$ and converged well for both positive and negative values of ϵ, for various Prandtl numbers. Although buoyancy coupling had some effect on the curves of figure 4 for $n = 0$, the effect was not significant enough to result in neutrally stable or amplifying solutions, even for large R.

Asymmetric disturbances ($n = 1$). This mode was shown to be unstable by Batchelor & Gill and by Kambe for the assumed top-hat and parabolic profiles. Our numerical solution of the governing equations for $n = 1$ has several points in common with the numerical schemes described above for $n = 0$. For buoyancy coupling and $n = 1$ we have an eighth-order, two-point boundary-value, eigenvalue problem. The numerical procedure is to integrate (40)–(42) separately, using the four sets of starting values determined from the expansions at $\eta = 0$ (i.e. equations (53)–(55)), from $\eta = 0$ to $\eta = \eta_e$. The boundary conditions to be satisfied at the edge of the boundary layer are

$$T(\infty) = S(\infty) = T'(\infty) + S'(\infty) \to 0. \tag{64}$$

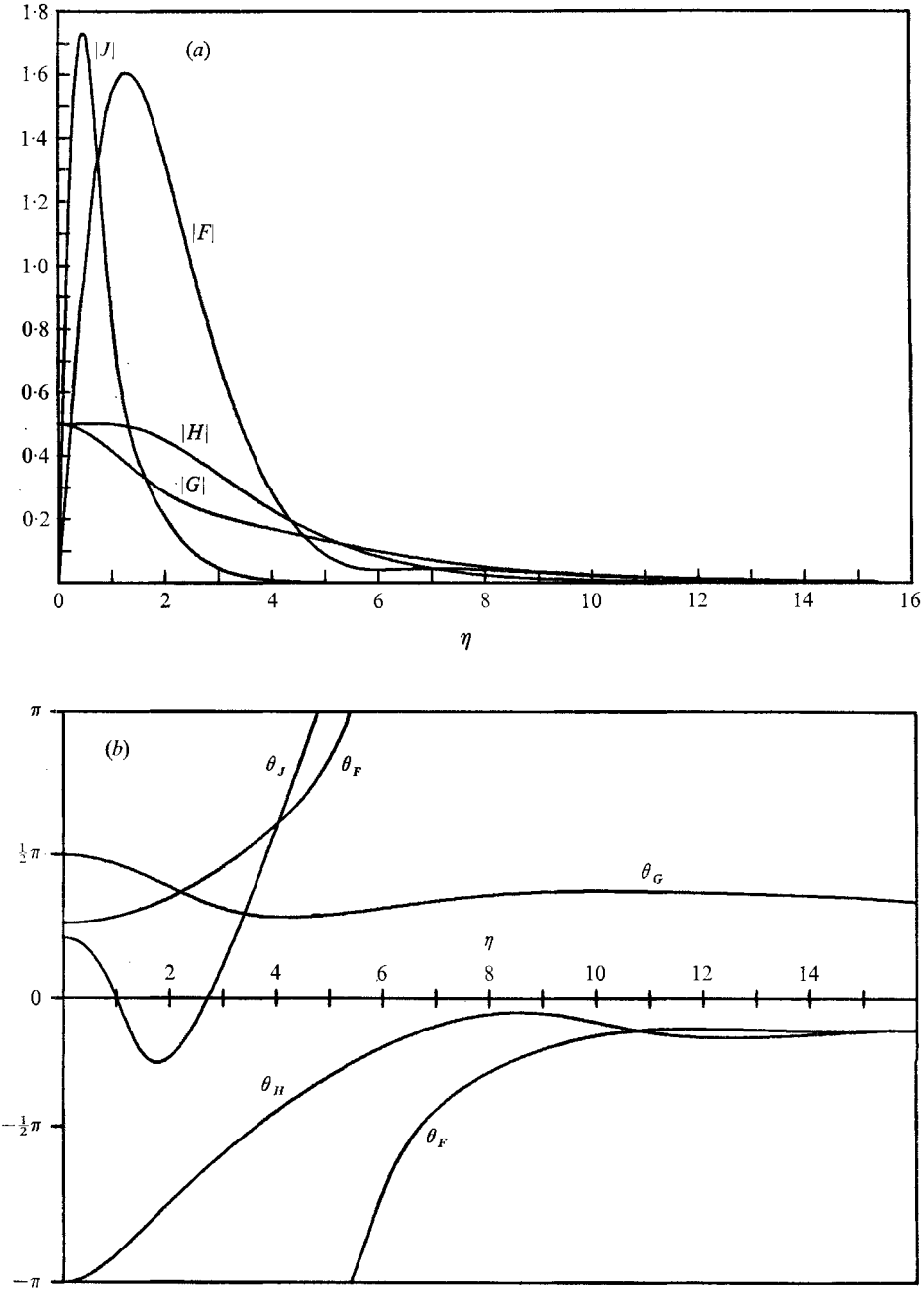

FIGURE 5. (*a*) Neutrally stable eigenfunctions and (*b*) corresponding phase angles for a non-buoyant jet ($\epsilon = 0$) and the disturbance mode $n = 1$. $R = 9{\cdot}4$, $\beta = 0{\cdot}10$, $\alpha_r = 0{\cdot}2206$, $\alpha_i = 0{\cdot}0000797$.

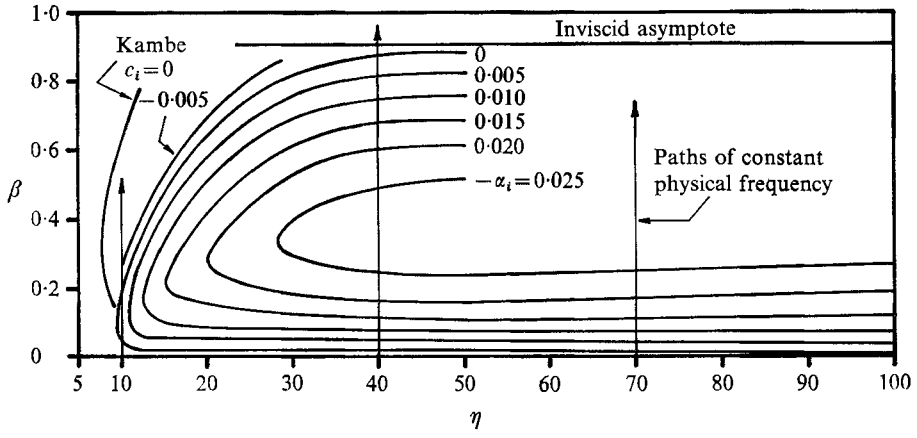

FIGURE 6. Amplification contours for a non-buoyant jet ($\epsilon = 0$) and the disturbance mode $n = 1$, and Kambe's neutral curve for a parabolic profile. Paths of constant physical frequency.

As before, one of the constants can be set equal to one ($A \equiv 1$) and the total functions constructed (at $\eta = \eta_e$) from the separate integrations satisfy the following:

$$S_1 + BS_2 + CS_3 + DS_4 = 0, \tag{65}$$

$$T_1 + BT_2 + CT_3 + DT_4 = 0, \tag{66}$$

$$(S_1' + T_1') + B(S_2' + T_2') + C(S_3' + T_3') + D(S_4' + T_4') = 0, \tag{67}$$

$$J_1 + BJ_2 + CJ_3 + DJ_4 = 0. \tag{68}$$

Equation (67) corresponds to the boundary condition $u'(\infty) \to 0$, and was chosen to be satisfied by the proper choice of α. Equations (65), (66) and (68) are satisfied by solving for the constants B, C and D. Again we successively iterate on α and apply the same correction procedure as was used for $n = 0$. The method converges very rapidly, and the effect of different mesh sizes and values of η_e was explored. Typical values used were $\Delta\eta = 0{\cdot}10$ and $\eta_e = 7$ (for small βR, $\eta_e = 20$).

We shall first discuss the results for the non-buoyant ($\epsilon = 0$) case. Typical eigenfunctions at the critical Reynolds number are shown on figure 5 for $n = 1$. These functions have the same general shape as those found near neutral conditions by Knowles & Gebhart for natural convection flow adjacent to a vertical surface, except for the modification around and at $\eta = 0$ due to different boundary conditions.

Unlike the results for $n = 0$, a neutral curve and an amplifying region were easily found for $n = 1$. The stability plane is shown in figure 6 in terms of the dimensionless frequency β *vs.* the momentum-flux parameter R. Contours of the spatial amplification rate α_i are shown. Recall that the physical nozzle Reynolds number is given by

$$Re_D = aR, \tag{69}$$

where $a = 4$ corresponds to a top-hat velocity distribution at the nozzle and $a = 8/\sqrt{3}$ corresponds to a parabolic distribution, as from Poiseuille flow in the nozzle.

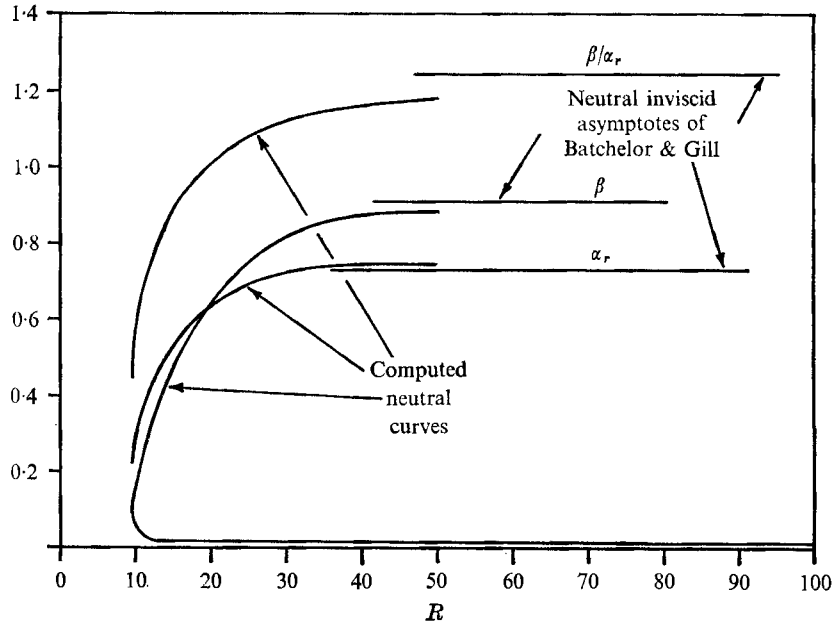

FIGURE 7. Various computed neutral curves approaching the neutral inviscid asymptotes of Batchelor & Gill for a non-buoyant jet ($\epsilon = 0$) and disturbance mode $n = 1$.

The neutral curve extends down to $R = 9{\cdot}4$. Its upper branch approaches the inviscid asymptote found by Batchelor & Gill for the same velocity profile. Recall that Batchelor & Gill's normalization for the base flow is different from that used here. However, the relation between β and the physical frequency is unaffected by these differences.

In figure 6 our neutral curve (for $n = 1$ and Schlichting's velocity distribution) is also compared with that of Kambe (for $n = 1$ and a discontinuous parabolic profile). Kambe did not relate his flow to a physical circumstance. However, if the velocity distribution satisfies a momentum-flux condition (as does Schlichting's) then his characteristic quantities are identical to those of Batchelor & Gill. The minimum unstable Reynolds number found by Kambe corresponds to $R = 8{\cdot}2$ (for $\beta = 0{\cdot}30$). The value we calculate is $R = 9{\cdot}4$ (for $\beta = 0{\cdot}1$), which agrees with the value calculated by Burridge. Figure 7 shows how our calculated wave speed, frequency and wavelength approach at large R the inviscid values (re-normalized) found by Batchelor & Gill.

An important physical interpretation of the stability plane deals with paths of constant physical frequency, as has been discussed by Dring & Gebhart (1968). As a small disturbance is convected downstream in the linear range in a given flow, its physical frequency remains constant. By using the characteristic length and velocity, one may determine its path, in any given flow, on a β *vs.* R plot.

From (12) and (13) we write the frequency f in terms of β, R and x as

$$f = \nu R^3 \beta / 2\pi x^2. \tag{70}$$

At constant frequency, β is seen to be proportional to x^2 in a given jet (ν, R).

Thus, the path of a disturbance of any frequency convected downstream in a given jet corresponds to increasing β at constant R. It moves up vertically on a β *vs.* R plot. Several such paths are shown on figure 6. A disturbance coming into the jet at small x may be initially in the stable region and then cross the neutral curve downstream to be amplified. For values of R less than that at the nose of the neutral curve, a small disturbance of any frequency will not be amplified as it is convected downstream. At larger R any small disturbance introduced into a jet at sufficiently small x will be damped until it reaches the lower branch of the neutral curve and then will begin to be amplified. Amplification continues until the disturbance reaches the upper branch of the curve. Then it will begin to be damped, provided that it has not become subject to nonlinear effects. This interpretation permits comparisons of these results with experiment.

An apparently careful experimental determination of the conditions for transition of round laminar jets was reported by Viilu. The transition range was found to lie between nozzle Reynolds numbers of 10·5 and 11·8. This corresponds to a momentum-flux Reynolds number R of about 3. The minimum value for instability calculated here is $R = 9{\cdot}4$. We do not now have a resolution of this difference. However, our calculations assume boundary-layer flow, which agrees with the complete jet solution for $R \gg 8$. Another difficulty in making such comparisons concerns the question of nonlinear effects and interactions. These effects are important with initially large disturbances and as any disturbance is highly amplified downstream. These matters are discussed in subsequent sections.

Comparisons with the laminar-length experimental results of Marsters, McNaughton & Sinclair and Reynolds requires more elaborate interpretation of our theoretical results. It is necessary to consider how disturbances grow. This is determined by calculating amplitude ratios and drawing their contours on the stability plane, in the manner of Dring & Gebhart. One computes the growth in amplitude of a small disturbance as it is convected downstream along a line of constant physical frequency in a given jet (ν, R). Assume that A_n is the amplitude of the disturbance as it crosses the neutral curve at x_n and $\hat{\alpha}_i(\hat{\beta})$ is the local spatial amplification rate. Then the amplitude A_x at x is found by integrating the following expression, from x_n to x:

$$\int_{A_n}^{A_x} \frac{dA}{A} = -\int_{x_n}^{x} \hat{\alpha}_i(x)\, dx. \tag{71}$$

In generalized form this becomes

$$\frac{A_x}{A_n} = \exp\left\{-\frac{R}{2}\int_{\beta_n}^{\beta_x} \alpha_i \frac{d\beta}{\beta}\right\}. \tag{72}$$

The ratio A_x/A_n is a measure of the relative amplitude of disturbances at downstream locations.

Lines of constant A_x/A_n, called amplitude-ratio contours, are shown on figure 8 for the asymmetric disturbance $n = 1$. If the disturbance has an amplitude of 1·0 at the lower branch of the neutral curve its amplitude is given by these contours as it is convected downstream.

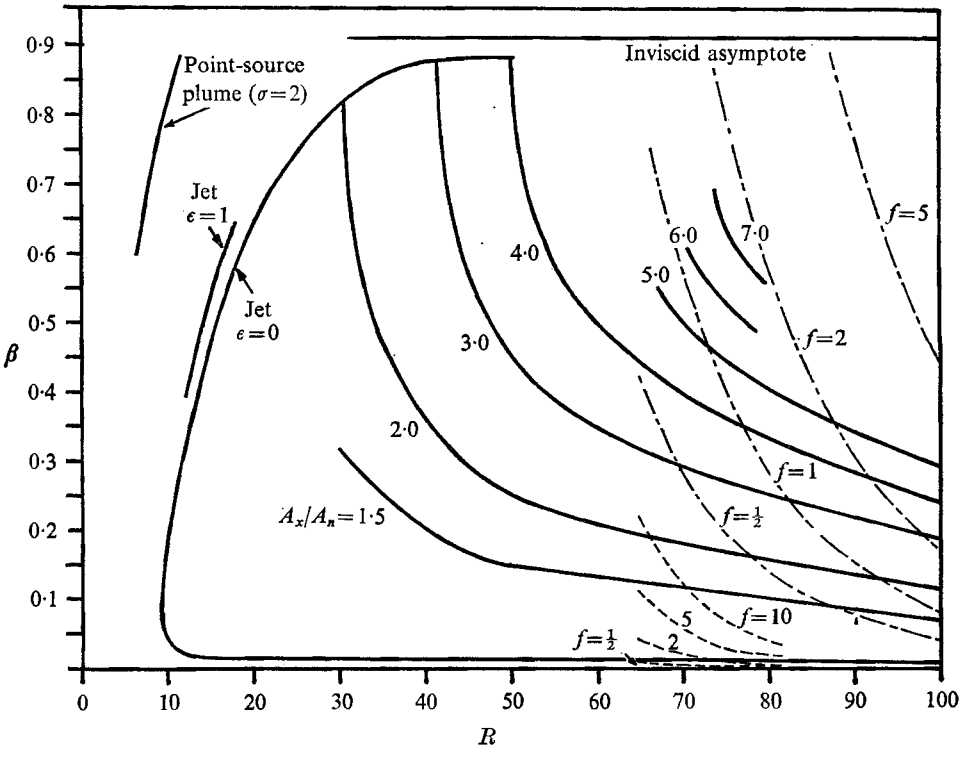

FIGURE 8. Neutral curve and amplitude-ratio contours for non-buoyant jet ($\epsilon = 0$). Neutral curve for a slightly buoyant jet $\epsilon = 1$ ($\sigma = 6{\cdot}7$) and for a thermal point-source plume for the disturbance mode $n = 1$ ($\sigma = 2$). ------, data of Reynolds for assumed frequencies; ——, our L/D data for buoyant jets for assumed frequencies.

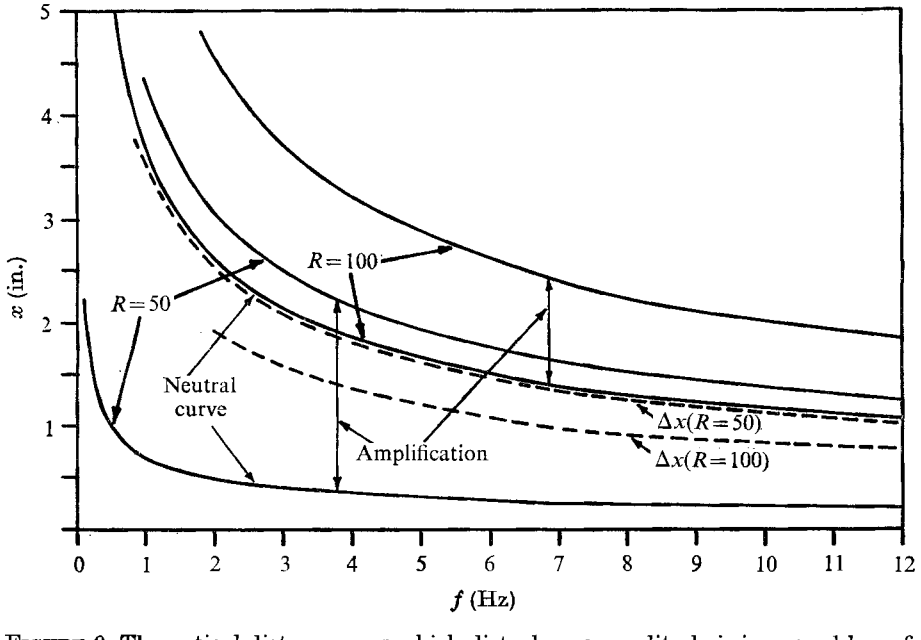

FIGURE 9. Theoretical distance over which disturbance amplitude is increased by a factor of 4 for water at 100 °F and the disturbance mode $n = 1$.

We see that all small disturbances in a given jet (ν, R) undergo the same increase in amplitude over the same range of β, independent of the frequency of the disturbance. However, the downstream distance over which this increase in disturbance amplitude occurs is a function of the disturbance frequency. From (70) the relation between a change in x and in β is

$$x_2 - x_1 = \Delta x = (\nu R^3/2\pi f)^{\frac{1}{2}} (\beta_2^{\frac{1}{2}} - \beta_1^{\frac{1}{2}}), \tag{73}$$

where Δx is the distance travelled in going from β_1 to β_2. Thus we see on figure 8 that for $R = 50$ a disturbance of any frequency will increase in amplitude by a factor of four as it travels between the lower and upper branch of the neutral curve. However, the actual distance Δx in the jet over which this increase in amplitude takes place is inversely proportional to the square root of the physical frequency. Thus higher frequencies are favoured for amplification.

Equation (73) has been used to plot figure 9 for $R = 50$ and 100. The curves are the two branches of the neutral curve as a function of x and frequency for water jets at 100 °F. Also shown is Δx, for an amplitude ratio of 4·0, for each value of R. The lower the frequency, the further a disturbance must be convected for the same amount of amplification. Also, a disturbance of given frequency is amplified by the same amount in a shorter distance Δx as the Reynolds number increases. This is consistent with the observations of previous investigators that the laminar length L of a jet before transition decreases with increasing Reynolds number. The experimental correlations suggested are of the form

$$L/D = A Re_D^B. \tag{74}$$

Our experimental laminar-length correlation and that of McNaughton & Sinclair are given later as equations (78) and (76), respectively. Since $x_1, \beta_1 \ll x_2, \beta_2$ we approximate Δx and $\Delta\beta$ by x_2 and β_2, and our relation from theory, equation (73), may be written as

$$x/D \approx R^{\frac{3}{2}} (\nu/2\pi f D^2)^{\frac{1}{2}} \beta^{\frac{1}{2}}. \tag{75}$$

Since x is the co-ordinate along the axis of the jet, this relation can be compared with experimental results of the form (74). We assume that the disturbance frequency remains constant and ask whether transition is related to amplitude-ratio contours, as it is known to be in some other flows. For agreement between equations (76) and (78) and equation (75), β at transition must be proportional to $R^{-7\cdot92}$ and $R^{-5\cdot24}$, respectively. Note that this required R dependence of β is approximately the same for the data of Reynolds, Marsters and McNaughton & Sinclair since the slopes are all about the same on an L/D *vs.* Re_D plot. The constant of proportionality is a function of the fluid, the diameter of the jet and the transition frequency. Our experimental, naturally occurring transition results and those of Reynolds (of the form (74)) are written in terms of β via (75) for assumed transition frequencies of 0·5, 2·0, 5·0 and 10·0 Hz. The results are shown on figure 8. Note that the data of Reynolds (presumably non-buoyant) is close to the lower branch of our theoretically determined neutral curve. This indicates that the applicable range of the theory corresponds to very low values of A_x/A_n. Our buoyant jet data are deeper into the amplified region, and correspond to

lower L/D's but higher L's. Recall that these computed results are for non-buoyant jets and that amplitude-ratio contours and paths of constant physical frequency are not at present known for buoyant jets. Hence, our buoyant jet data are not completely consistent with this theory. Neither set of curves coincides with amplitude-ratio contours, but they do have similar characteristics. They suggest that the theory has some relevance.

It was suggested by Hieber & Gebhart that transition for natural convection adjacent to a vertical surface occurs when $A_x/A_n \approx e^{10}$. Our experiments, described in following pages, indicate that the amplitude ratio corresponding to jet transition is very much lower than this, the typical value being less than $A_x/A_n = 4$. Apparently the difference is in the highly stabilizing influence of a surface, absent in free-boundary flows. A very low transition threshold was also indicated by the experiments of Pera & Gebhart (1971) in natural convection plumes arising from line sources.

3. Experiment

3.1. *Experimental apparatus*

The main components of our experimental apparatus were a 20 cm Mach–Zehnder interferometer, the water tank or test section, and the jet-producing device described in appendix B. Design considerations for this device were accuracy and ease of measuring the nozzle exit velocity, reproducibility of data, ease of taking data over a wide range of conditions and freedom from vibration. The most commonly used method of producing liquid-into-liquid jets has been simply gravity feed. Our jets were produced by a remote-controlled electrically driven pushing apparatus which could be operated in a cyclic fashion.

The jets were injected vertically into a large ($2 \times 2 \times 3$ ft inside dimension) stainless-steel tank insulated with polyurethane foam. The jet delivery tubing outside the tank was insulated with conventional insulation to prevent heat losses. However, the portion of the delivery tubing under water, as well as the nozzle, had double glass walls with the inside surfaces silvered and the gap evacuated to make the walls nearly adiabatic. This was essentially Dewar piping. The purpose was to reduce to the minimum any buoyancy-induced circulations in the test tank. Provision was made to use nozzles of various diameters by using conventional ground-glass fittings. The nozzles converged at the outlet, ensuring an almost uniform velocity profile. Thermocouples were placed in the nozzle near the exit, further upstream in the delivery tubing, and in the tank water away from the jet. Thermocouple outputs were recorded on a dynograph.

The tank was equipped with interferometer grade windows and the temperature field of the heated round jets was observed using a new 20 cm Mach–Zehnder interferometer similar to the one described by Gebhart & Knowles (1966). A 20 mW helium–neon gas laser was used as a light source to avoid the need for a compensation chamber. The resulting interferograms (see figures 12–14, plates 1–3, for example) are inevitably of lower quality than those which result from the use of less coherent light. They were recorded with a 35 mm single-lens-reflex camera.

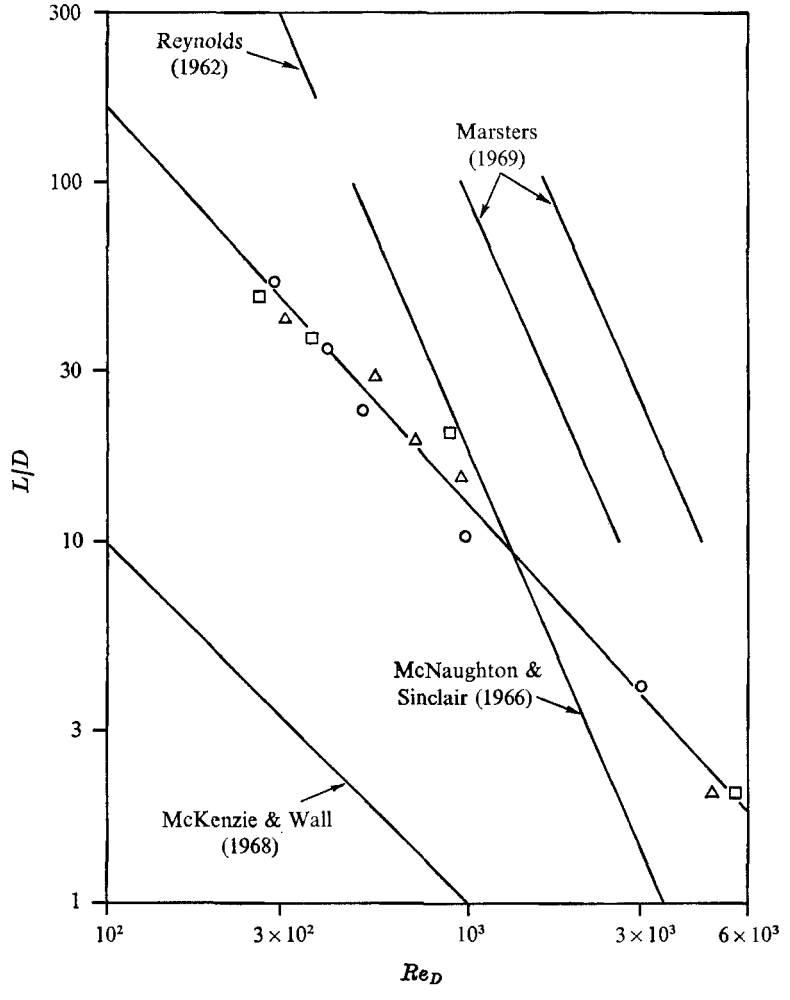

FIGURE 10. Experimental laminar-length data for buoyant jets and correlations of the data of other investigators. ○, Δt = 20 °F; △, Δt = 30 °F; □, Δt = 45 °F.

3.2. *Effect of buoyancy on laminar length*

A common experimental approach to jet stability is to measure the laminar jet length as a function of the Reynolds number. The observations of Reynolds, McNaughton & Sinclair, Marsters and McKenzie & Wall are in this form. The data are displayed on a log–log plot of the laminar length divided by the diameter of the jet, L/D, *vs.* the jet Reynolds number. Attempts at correlation take the form of straight lines on this plot.

The suggestion of Marsters for $Re_D < 2300$ is given by (74). The data of Reynolds and of McNaughton & Sinclair suggest

$$L/D = 10^8 Re_D^{-2.46}. \tag{76}$$

This Reynolds number dependence is about the same, but the constant differs by a factor of 10. This might suggest that the Marsters data were taken in quieter

surroundings. The experimental results of McKenzie & Wall are correlated as follows:

$$L/D = 10^3 Re_D^{-1}. \tag{77}$$

This is a very large difference. Marsters notes this discrepancy, but does not offer an explanation. All the results are compared in figure 10.

Our measurements of laminar length are also shown in figure 10. A typical interferogram showing transition is shown in figure 14 (*b*) (plate 3). The correlating line for our data shown in figure 10 is

$$L/D = 3 \times 10^4 Re_D^{-1{\cdot}12}. \tag{78}$$

The values of temperature difference shown on the figure are $\Delta t = t_j - t_\infty$.

McKenzie & Wall's correlation has the same Reynolds number dependence as that of our data. However, the level is different by a factor of 30. It is unfortunate that McKenzie & Wall do not adequately describe their experiment. They refer to the working fluids as either gas or liquid and make no mention of which gas or what liquid. However, schlieren and birefringent flow visualization techniques were used and it appears that the jets were injected horizontally. Since density-sensitive optical devices were used, the jets were obviously buoyant. Jets in the low Reynolds number range 10–1000 are now known (Mollendorf & Gebhart 1973) to be sensitive to buoyancy effects. Recall the definition $\epsilon(x) = Gr/R^4$. Although the degree of buoyancy can only be guessed for their experiments, it appears that their very low L/D values are either the result of significant buoyancy effects, horizontal injection, a high disturbance level or a combination of these. The lack of documentation makes any further conjecture impossible.

In our experiments it was possible to determine the laminar length and also to investigate the effects of varying amounts of thermal buoyancy on the laminar length. Data were taken for a range of Reynolds numbers of from 300 to 5500 for jet–ambient temperature differences of 20, 30 and 45 °F. Our data on figure 10 have a slope very different from those of the correlations in (74) and (76). Our higher Reynolds number data cross the region of McNaughton & Sinclair.

Marsters was concerned about buoyancy effects. He calculated $Gr_{D,\Delta\rho}/Re_D^2$ for his experiments to be 2×10^{-4} and concluded that such effects were small. This is a very approximate calculation. The appropriate characteristic quantities are not nozzle diameter and exit velocity, but are given by (12) and (13). The perturbation parameter $\epsilon(x) = Gr/R^4$ is the appropriate measure of the effects of buoyancy. Marsters' experiments in CO_2 had negative ϵ. A typical value would be about $-0{\cdot}1$.

Values of ϵ at the transition point, $\epsilon(L)$, were calculated for our buoyant-jet data. The results are shown in figure 11 as a plot of L/D *vs.* $\epsilon(L)$, which varied from $3{\cdot}2 \times 10^{-5}$ to $1{\cdot}69 \times 10^{+2}$ over the range of Reynolds numbers we studied. The laminar-length data are seen to correlate well with $\epsilon(L)$ as follows:

$$L/D = 2{\cdot}12[\epsilon(L)]^{0{\cdot}214}. \tag{79}$$

The data above $\epsilon(L) = 1$ have more scatter. This is thought to be due to the unsteadiness of the observed point of jet transition under such highly buoyant conditions. Such flows are more nearly thermal plumes of very different stability

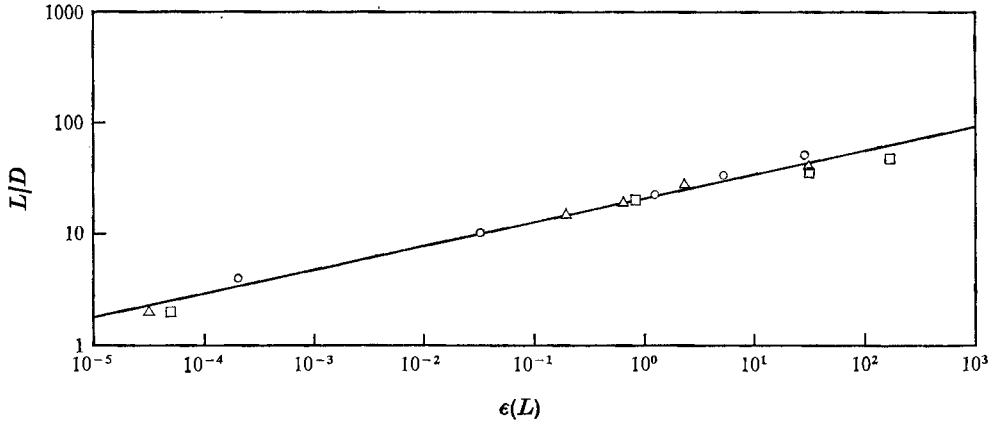

FIGURE 11. Laminar-length data for a buoyant jet as a function of relative buoyancy. ○, $\Delta t = 20$ °F; △, $\Delta t = 30$ °F; □, $\Delta t = 45$ °F.

characteristics. The transition location was clearly defined and steady at smaller values of ϵ. Our attempt to correlate transition data with $Gr_{D,\,\Delta t_j}/Re_D^2$ was unsuccessful. The data grouped themselves according to values of Δt.

The above correlation can be used with the definition of ϵ to arrive at the following empirical result for the laminar length of a buoyant jet:

$$L/D = 568{\cdot}5[(2\sigma+1)\,Gr_{D,\,\Delta t_j}/Re_D^3]^{\frac{1}{8}}. \tag{80}$$

This form is clearly at complete variance with previous supposedly non-buoyant correlations.

The excellent correlation from figure 11 and its corollary, equation (80), results in a quandary. A non-zero asymptote for L/D *vs.* Re_D is not found as $\epsilon(L) \to 0$, i.e., as $Gr_{D,\,\Delta t_j} \to 0$. This characteristic thus questions the concept that the transition location is a function of Re_D as well as the relation between stability theory and actual jet transition. Our experimental results do not guide us to a resolution of these conflicts. The data on figure 11 simply do not approach an asymptotic value at small $\epsilon(L)$. This remains a mystery. Nevertheless, our subsequently discussed measurements of controlled disturbance growth in low buoyancy jets are in agreement with the predictions of stability theory and the measured laminar lengths are also consistent with it.

3.3. *Artificially induced disturbances*

In order to assess the detailed predictions of stability theory, we carried out an experimental investigation of the behaviour of artificially induced disturbances of controlled frequency. For several kinds of natural convection flow, similar experiments have indicated the range of validity of this kind of analysis, substantiated many of its details and have also given insight into the later processes toward transition.

The flow in jets and plumes differs from natural convection over a vertical surface not only because of the absence of the stabilizing influence of the plate, but also in the variation of their energy content. Flows over heated surfaces are

continually fed with thermal energy and their momentum continually increases up the surface. Jets and plumes contain constant amounts of thermal energy, and jets have unchanging momentum if there are no buoyancy forces in the flow field. Thus, the velocity in these free-boundary flows does not increase downstream. This characteristic may cause the complicated modes of jet instability and transition which have been reported.

A series of interferograms showing some of the characteristics of naturally occurring jet breakdown is shown in figures 12–14 (plates 1–3). All conditions, other than the jet Reynolds number, are essentially the same. At the lower Reynolds numbers the jets tend to meander periodically and twist in a wavelike manner. It seems they would more rapidly suffer severe disruption if the flow contained more energy. As the Reynolds number increases, the twisting is more violent and the wavelike meandering occasionally degenerates into what appears to be turbulent bursts. At yet higher Reynolds numbers the laminar regions and transition zone are shortened and the familiar, relatively fine-grain turbulent flows are quickly produced.

Disturbance formulations in stability analysis suggest that one might categorize disturbances on the basis of their symmetry. Naturally occurring symmetric disturbances are seen in figure 14(*a*) at $Re_D = 537$. However, the symmetric lumps near the nozzle outlet quickly distort into non-symmetrical form. In the theory, the former are much more stable than the latter.

The predicted stability of symmetric disturbances was tested experimentally. A short length of flexible surgical tubing was inserted into the jet delivery line, between the nozzle and an upstream check valve. Small amplitude oscillations were applied to the tube by subjecting an electromagnet to a modulated d.c. voltage, in the manner of Knowles & Gebhart. Over a wide range of frequencies and jet Reynolds numbers such oscillations had very little effect on jet stability. The symmetrical disturbances were seen to damp out. The flow reacted noticeably only when very large amplitudes were used.

Controlled asymmetric disturbances were introduced with a vibrating ribbon. The ribbon, of $\frac{1}{16}$ in. high × 1 in. wide × 0·0005 in. thick inconel foil, was supported by a long rod pivoted at its centre. The other end of the rod was connected to the electromagnetic vibrator. The electromagnet was equipped with a calibrated linear transducer converter, permitting the measurement of disturbance amplitude. The resonant frequency of the rod (including the weight of the extension arm) was calculated to be 12·5 Hz. The ribbon was positioned across the axis of the jet. The effect of the presence of the stationary ribbon in the flow was checked (by comparing interferograms with and without the vibrator in the flow field) and found to be undetectable.

The asymmetric disturbances were highly destabilizing. Data were taken for a range of Reynolds numbers, frequencies and vibrator amplitudes. Although much of the data is for buoyant jets, some approximately non-buoyant flows were also studied. The results are presented as collected interferograms on figures 15–20 (plates 4–9). The frequency and amplitude of the ribbon are given below each photograph. The local value of the perturbation parameter $\epsilon(x)$ is shown to the right of the interferograms of the undisturbed flow. The numbers

to the right of the jets subjected to a particular frequency are the local values of the amplitude ratios calculated from (72) and shown on figure 8. The points at which each jet crosses the lower and upper branches of the neutral curve are indicated by N.C. The location of the inviscid asymptote is indicated by I.V.N.C.

Downstream distances were converted to values of β, via (70), by taking $x = 0$ to be at the nozzle exit. This is not strictly correct since the theory supposes that the flow originates from a point source of momentum. Although these flows show boundary-layer characteristics, the nozzles are far from being point sources. This effect could perhaps be treated by considering a virtual source at some distance below the nozzle exit. Its proper location might be conjectured from quantitative velocity or temperature measurements at the nozzle exit. However, this was not attempted and the seriousness of this problem is not known.

This collection of data shows interesting characteristics when compared with computed stability characteristics. The jet shown in figure 15, for $Re_D = 138$ ($R = 30$, for flat profile), is very buoyant and is more like a point-source plume than a jet. Note that N.C. also corresponds to $A_x/A_n = 2$ for this Reynolds number. Neither frequency nor amplitude have appreciable effects. Jet breakdown always occurs about 5 in. downstream and the transition zone is not well defined. This is consistent with our calculations for non-buoyant jets since at $R = 30$ the amplification rates are very small. The large undulations seen are clearly not in a linear range. The initial instability is probably entirely a plume mode.

The jet of figure 16, for $Re_D = 250$ ($R = 54$), is less buoyant, but still is very buoyant. This jet is calculated to be subject to much higher amplification rates. The flow undergoes transition earlier and the location is more clearly defined. The ribbon lies approximately at the lower branch of the neutral curve for these frequencies.

The jet of $Re_D = 316$ ($R = 68$) in figure 17 has still less relative buoyancy. Although this flow has higher momentum, the reduction in buoyancy apparently inhibits transition, except at higher frequencies, for which disturbances are calculated to undergo the same amplification over much shorter distances. Note that, at lower frequencies, the vibrator is below the neutral curve and at higher ones is in the unstable region. The higher frequency disturbances are not initially subject to damping and are seen to amplify very rapidly.

This was further explored at a slightly higher Reynolds number $Re_D \approx 370$ ($R = 80$) as shown in figure 18. The vibrator was raised 1 in. The vibrator is now in the calculated unstable region for all frequencies used. All disturbances seem to undergo immediate amplification. This observation and the one above, that disturbances introduced at values of β below the theoretical neutral curve are initially damped, seem to verify experimentally the existence of the calculated lower branch of the neutral curve.

Data at $Re_D = 481$ ($R = 104$) are shown on figure 19. Again the vibrator is always in the amplified region and disturbances of all frequencies are amplified very quickly. Note that transition occurs at shorter downstream distances as the frequency increases. Similar behaviour is seen in figures 17 and 18. This agrees with our theoretical prediction that $x^2 \propto 1/f$.

Figure 20 is for $Re_D = 537$ ($R = 116$) and a very low level of buoyancy. Transition quickly occurs for no vibration and for all frequencies. We suspect that this vigorous flow was subject to additional disturbances of large amplitude. These perhaps arose in the jet-production system at this high delivery rate.

4. Summary and conclusions

The effects of small amounts of thermal buoyancy on laminar jet flow had been previously determined analytically. The principal effects were found to be an increase in the axial component of the velocity and a thinning of the jet by the change in pressure field which resulted from this alteration of the velocity. The magnitude of these effects is small but the trends are clear and are consistent with physical reasoning, and with the observations of McNaughton & Sinclair.

The hydrodynamic stability of laminar jets has been investigated both analytically and experimentally, including some effects of buoyancy. The non-buoyant jet stability equations were solved numerically using the proper boundary-layer base flow for both symmetric and asymmetric disturbances. It was found that asymmetric ($n = 1$) disturbances are amplified over shorter distances as the frequency and Reynolds number increase. Calculated eigenfunctions show the same characteristics as those found for other flows. Damped eigenvalues correspond to more 'flowery' eigenfunctions, simpler ones are found for conditions near neutral. Consequently, the disturbance shear stress is less well behaved as $\alpha_i > 0$.

We did not find a neutral curve for symmetric ($n = 0$) disturbances. Such a curve was found for the first asymmetric ($n = 1$) one. This is consistent with the inviscid results of Batchelor & Gill in that neutral or amplifying disturbances were not found for $n = 0$. Our computed neutral curves (disturbance wave speed, frequency and wavelength) approach the neutral inviscid asymptotes of Batchelor & Gill at large R. The neutral curve found by Kambe for a 'discontinuous parabolic' profile lies at lower R than that calculated here using the proper velocity profile. This less stable condition is perhaps due to the discontinuity of the parabolic profile.

Spacewise amplification characteristics were determined. Then the effect of jet buoyancy on stability was determined from the coupled stability equations for very small amounts of buoyancy and the neutral stability curve was found to lie at slightly lower R (for the same β). This amount of buoyancy slightly destabilizes the flow. The stability of the extreme case of buoyancy in an axisymmetric flow, the point-source thermal plume, was then determined for $\sigma = 2$. From figure 8, the neutral curve is seen to lie at even lower $R \equiv (\frac{1}{4}Gr)^{\frac{1}{4}}$ than that of the jet. Even though these results lie below the applicable range of boundary-layer theory, they indicate that large buoyancy effects drastically destabilize the flow. The stability predictions for plume flow are consistent with previous results for plane plumes. We conclude that the buoyancy mechanism of energy exchange between the base flow and disturbances is very important in jets having large buoyancy.

The destabilizing influence of a large level of thermal buoyancy was also

observed experimentally. Our experimental laminar-length (transition) observations for jets show that increasing amounts of aiding thermal buoyancy cause the jets to undergo transition at much shorter downstream distances. The data were found to correlate with our theoretically determined buoyancy perturbation parameter.

Controlled disturbances were introduced into jets having different and large amounts of buoyancy. Such flows have not yet been analysed and, therefore, no stability predictions are possible. We do not yet even know the paths such disturbances follow on a stability plane.

Although our experiments do not strictly simulate the conditions of non-buoyant jet flow, the results are at least consistent with stability theory. The experiments tend to support the existence of a lower branch of the neutral curve. They also indicate that transition to turbulence occurs at very much lower values of the amplitude ratio than for the natural convection adjacent to a vertical surface. This is consistent with findings for another free-boundary flow previously studied, the plane plume. We also found that highly buoyant jets apparently undergo transition by a non-jet mechanism which is presumably more like that to which a point-source plume is subject.

The exact size of the amplitude ratio where one might expect turbulence might depend on the size of the disturbance and the point of its introduction. Nevertheless, we found that the jets having small buoyancy became turbulent for calculated non-buoyant amplitude ratios of about 4. This is also a test of the predicted effect of disturbance frequency. We found that transition occurs at shorter downstream distances as the frequency increases. In addition, we found that symmetric disturbances did not amplify, in accordance with the predictions of theory.

The authors wish to acknowledge the support of this research by the National Science Foundation under Research Grant GK18529. The first author also wishes to acknowledge the above agency for support as a Research Assistant under the same grant and for National Science Foundation support as a Graduate Trainee. The authors also wish to acknowledge helpful discussions with colleagues, especially those with Prof. S.-F. Shen. Prof. C.A. Hieber, Dr T. Audunson and Dr Y. George.

Appendix A

Consideration of the buoyancy perturbation parameter $\epsilon(x)$ indicates that the relative magnitude of the buoyancy force compared with that of the momentum force increases downstream; recall that $\epsilon \propto x^2$. Thus, a round buoyant jet will tend to assume the characteristics of thermal point-source plumes downstream. The point-source plume, therefore, is the limiting case of a buoyant jet. Because of this, some consideration will be given to the thermal point-source plume.

The point-source plume was analysed by Schuh (1948) using boundary-layer approximations for $\sigma = 0{\cdot}7$. Closed-form solutions were found by Yih (1951) for $\sigma = 1$ and 2. The basic governing equations and boundary conditions for the

point-source plume are the same as for a round jet. For the plume, momentum flux is not conserved. However, if there are no heat sources in the flow field, the following heat-flux condition applies:

$$Q \equiv \int_0^\infty 2\pi\rho c_p(t-t_\infty)uy\,dy = \text{constant}. \tag{A 1}$$

A similarity analysis proceeds by taking $\eta = yb(x)$, $\psi = c(x)f(\eta)$ and $d(x) = t_0 - t_\infty$. The x functions are determined as

$$b(x) = (\tfrac{1}{4}Gr_{x,\,\Delta t_0})^{\frac{1}{4}}/x, \tag{A 2}$$

$$c(x) = x, \quad d(x) = Nx^{-1}. \tag{A 3), (A 4}$$

The governing equations become

$$\left(f'' - \frac{f'}{\eta}\right)' = \frac{ff'}{\eta^2} - 4\eta\phi - \frac{ff''}{\eta}, \tag{A 5}$$

$$(\eta\phi' + \sigma f\phi)' = 0. \tag{A 6}$$

By comparing these equations with those for a jet, it can be seen that the only difference is in the second term on the right-hand side of (A 5). Note also that the η's are different. From (A 6) for $\sigma = 2$ we have

$$4\eta\phi = f'^2/\eta. \tag{A 7}$$

This makes (A 5) the same as that for a non-buoyant jet. The plume solutions are

$$f(\eta) = \eta^2/(1+\tfrac{1}{4}\eta^2) \tag{A 8}$$

and

$$\phi(\eta) = (1+\tfrac{1}{4}\eta^2)^{-4}. \tag{A 9}$$

Consequently, the point-source plume and the round jet have the same non-dimensional velocity and temperature fields for $\sigma = 2$. The stability analysis proceeds as before with the exception of the characteristic quantities. For the plume, they are

$$L_c = x/(\tfrac{1}{4}Gr_{x,\,\Delta t_0})^{\frac{1}{4}}, \tag{A 10}$$

$$V_c = \nu(\tfrac{1}{4}Gr_{x,\,\Delta t_0})^{\frac{1}{4}}/x, \tag{A 11}$$

$$T_c = t_0 - t_\infty. \tag{A 12}$$

The stability equations for the point-source plume are identical to those for the buoyant jet for $\sigma = 2$, if we consider

$$R = (\tfrac{1}{4}Gr_{x,\,\Delta t_0})^{\frac{1}{4}} \tag{A 13}$$

and

$$\epsilon = 4. \tag{A 14}$$

Note that (A 13) and (A 14) are a direct consequence of (A 10) and (A 11).

The computer programs for the stability of a buoyant jet are used for the point-source plume by taking $\sigma = 2$ and $\epsilon = 4$ and neglecting the ϵ corrections to the base flow. This was done and a portion of the neutral curve for a point-source plume with $\sigma = 2$ is shown on figure 10 for the mode $n = 1$. Note also that the non-buoyant jet ($\epsilon = 0$) stability results are exactly the same as those for the point-source plume for $\sigma = 2$ if coupling through buoyancy is neglected. From (A 10) and (A 11) the lines of constant physical frequency are given by

$$\beta \propto (\tfrac{1}{4}Gr_{x,\,t_0})^{\frac{1}{4}}. \tag{A 15}$$

These are represented by a family of straight lines passing through the origin on a β *vs.* $(\frac{1}{4}Gr_{x,\,\Delta t_0})^{\frac{1}{4}}$ plot. This is similar to the line-source plume result of Pera & Gebhart (1971) (and the jet result discussed above) in that convected disturbances traverse the unstable region to emerge again into stable conditions. The jet flows with considerable buoyancy are much more complicated. The lines of constant physical frequency are thought to lie between the two limiting cases of non-buoyant jets and point-source plumes.

Appendix B

The base for the pumping apparatus is a 9×48 in. steel channel upon which the various components were mounted. A $\frac{1}{15}$ h.p., 110 V, 60 cycle, a.c. synchronous motor operating at 1800 r.p.m. was connected to a positive-drive reversible gear box. The output from the gear box could be continuously varied between 0 and 400 r.p.m. This rotary motion was used to turn a 1 in. heavy-duty micrometer head. The micrometer was fixed to the channel base at one point but a collar allowed it to slide at the point of attachment to the gear box. The rotary motion of the gear box was converted to linear displacement at the rate of $\frac{1}{40}$ in. per revolution as the micrometer rotated. This pushing apparatus was mounted on foam-rubber supports and placed in an adjacent room to minimize vibrations.

The micrometer pushed a $2\frac{1}{4}$ in. diameter hydraulic cylinder by means of a point-contact mounted ball bearing. This cylinder was connected to a $\frac{15}{16}$ in. diameter hydraulic cylinder by means of flexible high pressure hose. A special blend of silicone oil was used as a working fluid and the hose was slightly coiled and clamped to the wall to eliminate vibrations. Air was removed from the hydraulic lines by means of bleeder valves. The smaller cylinder was mounted on a 3 in. aluminium channel near the test section and had a stroke of about 6 in. It was connected to a 30 ml glass hypodermic syringe. The syringe was connected with a glass tee to both a controlled-temperature bath and the nozzle of the jet, with teflon tubing. Two check valves were used. When the syringe was loading with hot water it did not draw water from the test section but from the heated bath. During jet discharge into the test chamber, backflow into the hot water bath was prevented by the other check valve.

The driving part of the apparatus was equipped with adjustable micro-switches which are tripped when the micrometer is at its extremes of movement. The gear box had both forward and reverse as well as a neutral position, and could be set by moving a lever. Electromagnets were attached to this lever so that all three positions could be set by remote control. The gear box was designed to go from any of the three positions to any other while operating. When the apparatus was initially turned on the gear box was in neutral and set at a desired speed between 0 and 400 r.p.m. When the proper button was pushed, the gear box was put into reverse and the rotation was such that the syringe drew hot water into the tubing. Compressed air was used to push the cylinder back as the syringe loaded since the point-contact mounted ball bearing cannot pull back the large cylinder. When the micrometer reached the end of its stroke (i.e. the syringe was loaded) a microswitch was tripped and released the air pressure by

means of a three-way solenoid valve and at the same time threw the gear box into a forward gear. At this time there was flow through the nozzle. The jet flow continued until the micrometer tripped the other microswitch, which threw the gear box into neutral and thus ended the cycle. The entire cycle was repeated by simply pushing the start button. A motor was connected to the speed control shaft of the gear box and so the flow rate (and thus the Reynolds number) was continuously adjustable by remote control.

The angular velocity of the micrometer was measured by using a photodiode and a collar with 30 evenly spaced holes drilled around the circumference. A focusing light bulb was placed on one side of the collar and the photodiode on the other. The diode was placed in a circuit with a resistor and battery in such a way that an electrical signal was generated as the holes in the collar chopped the light. The motion between two successive signals corresponded to $\frac{1}{30}$ of a revolution of the micrometer.

The Reynolds number was calculated to be

$$Re_D = \left[\frac{1}{T\nu}\left(\frac{D_1}{D_2}\right)^2\left(\frac{D_s^2}{D_j}\right)\right]\Omega, \tag{B 1}$$

where Re_D is the nozzle exit Reynolds number based on the average velocity, T is the number of threads per inch of the micrometer, D_1 and D_2 are the diameters of the large and small cylinders, respectively, D_s and D_j are the diameters of the syringe and jet nozzle respectively, and Ω is the angular velocity. The fixed dimensions of the apparatus are as follows: $T = 40$ threads/in., $D_1 = 2{\cdot}25$ in., $D_2 = \frac{15}{16}$ in. and $D_s = 0{\cdot}923$ in. For water at 100 °F and for a $\frac{1}{8}$ in. nozzle diameter this relationship reduces to

$$Re_D = 30{\cdot}7N, \tag{B 2}$$

where N is the number of impulses per second. The impulses at the photodiode were counted with an EPUT meter using a typical gate time of 10 s. The signal was also observed using an oscilloscope and found to be essentially a square wave. The uniformity of the motion was checked by recording the signal on an Offner recorder for the entire length of the cycle. Although the amplitude of the signal varied slightly, the frequency remained constant. Photographs of the various components of the experimental apparatus are shown in Mollendorf (1971).

REFERENCES

ANDERSON, A. B. C. 1954 The jet-tone orifice number for orifices of small thickness–diameter ratio. *J. Acoust. Soc. Am.* **26**, 21.

ANDERSON, A. B. C. 1955 Structure and velocity of the periodic vortex–ring flow pattern of a primary Pfeifenton (pipe tone) jet. *J. Acoust. Soc. Am.* **27**, 1048.

ANDERSON, A. B. C. 1956 Vortex-ring structure-transition in a jet emitting discrete acoustic frequency. *J. Acoust. Soc. Am.* **28**, 914.

BATCHELOR, G. K. & GILL, A. E. 1962 Analysis of the stability of axisymmetric jets. *J. Fluid Mech.* **14**, 529.

BECKER, H. A. & MASSARO, T. A. 1968 Vortex evolution in a round jet. *J. Fluid Mech.* **31**, 435.

BURRIDGE, D. M. 1968 The stability of round jets. Ph.D. thesis, Bristol University.

CROW, S. C. & CHAMPAGNE, F. H. 1971 Orderly structure in jet turbulence. *J. Fluid Mech.* **48**, 547.

DRING, R. P. & GEBHART, B. 1968 A theoretical investigation of disturbance amplification in external laminar natural convection. *J. Fluid Mech.* **34**, 551.

GEBHART, B. & KNOWLES, C. P. 1966 Design and adjustment of a 20 cm Mach–Zehnder interferometer. *Rev. Sci. Instrum.* **37**, 12.

GILL, A. E. 1962 On the occurrence of condensations in steady axisymmetric jets. *J. Fluid Mech.* **14**, 557.

HIEBER, C. A. & GEBHART, B. 1971 Stability of vertical natural convection boundary layers: some numerical solutions. *J. Fluid Mech.* **48**, 625.

KAMBE, T. 1969 The stability of an axisymmetric jet with parabolic profile. *J. Phys. Soc. Japan*, **26**, 566.

KNOWLES, C. P. & GEBHART, B. 1968 The stability of the laminar natural convection boundary layer. *J. Fluid Mech.* **34**, 657.

LANDAU, L. D. & LIFSHITZ, E. M. 1959 *Fluid Mechanics*, p. 86. Pergamon.

MCKENZIE, C. P. & WALL, D. B. 1968 Transition from laminar to turbulence in submerged and bounded jets. *Fluidics Quart.* **4**, 38.

MCNAUGHTON, K. J. & SINCLAIR, C. G. 1966 Submerged jets in short cylindrical flow-vessels. *J. Fluid Mech.* **25**, 367.

MARSTERS, G. F. 1969 Some observations on the transition to turbulence in small, unconfined free jets. *Queen's University, Kingston, Ontario, Rep.* no. 1–69.

MOLLENDORF, J. C. 1971 The effect of thermal buoyancy on the hydrodynamic stability of a round laminar vertical jet. Ph.D. thesis, Cornell University.

MOLLENDORF, J. C. & GEBHART, B. 1973 Thermal buoyancy in round laminar vertical jets. *Int. J. Heat Mass Transfer*, **16**, 735.

PERA, L. & GEBHART, B. 1971 On the stability of laminar plumes: some numerical solutions and experiments. *Int. J. Heat Mass Transfer*, **14**, 975.

REYNOLDS, A. J. 1962 Observation of a liquid-into-liquid jet. *J. Fluid Mech.* **14**, 552.

SCHLICHTING, H. 1933 Laminare Strahlausbreitung. *Z. angew. Math. Mech.* **13**, 260. (See also 1955 *Boundary Layer Theory*, p. 181. McGraw-Hill.)

SCHUH, H. 1948 Boundary layers of temperature. *W. Tollimien's Boundary Layers*, §B6. Brit. Min. Supply, German Document Centre, Ref. 3220T.

SQUIRE, H. B. 1951 The round laminar jet. *Quart. J. Mech. Appl. Math.* **4**, 321.

VIGNES, M. 1968 Contribution à l'étude des jets gazeux verticaux dans une atmosphère calme. *Rev. Gén. Thermique*, **7**, 1205.

VIILU, A. 1962 An experimental determination of the minimum Reynolds number for instability in a free jet. *J. Appl. Mech.* **29**, 506.

YIH, C.-S. 1951 Free convection due to a point source of heat. *Proc. 1st U.S. Nat. Congr. Appl. Mech.* pp. 941–947.

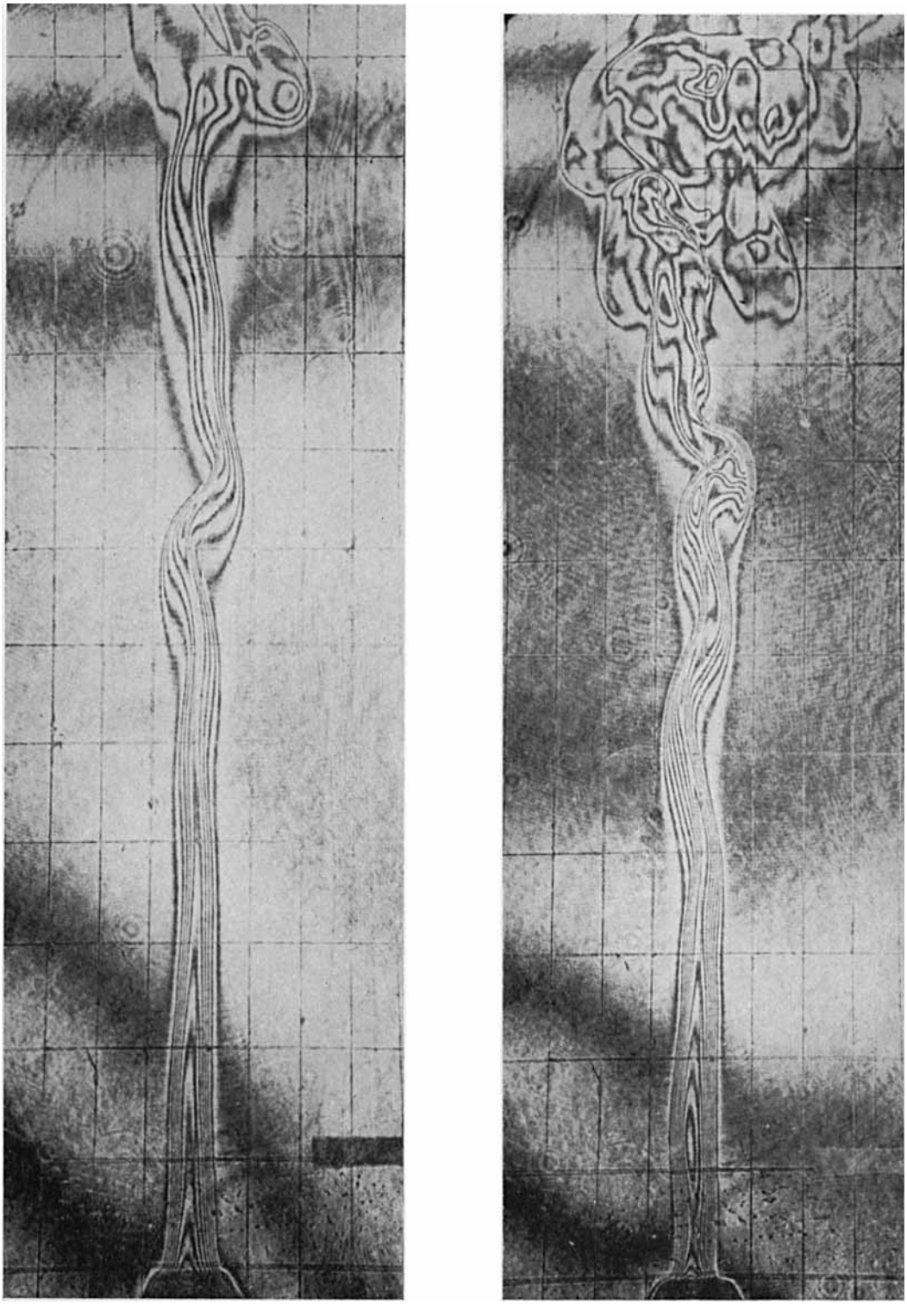

(*a*) (*b*)

FIGURE 12. Naturally occurring breakdown for (*a*) $Re_D = 138$ ($R = 30$), $t_j = 101$ °F, $t_\infty = 82$ °F and (*b*) $Re_D = 250$ ($R = 54{\cdot}2$), $t_j = 107$ °F, $t_\infty = 81$ °F, $D = \frac{1}{4}$ in.

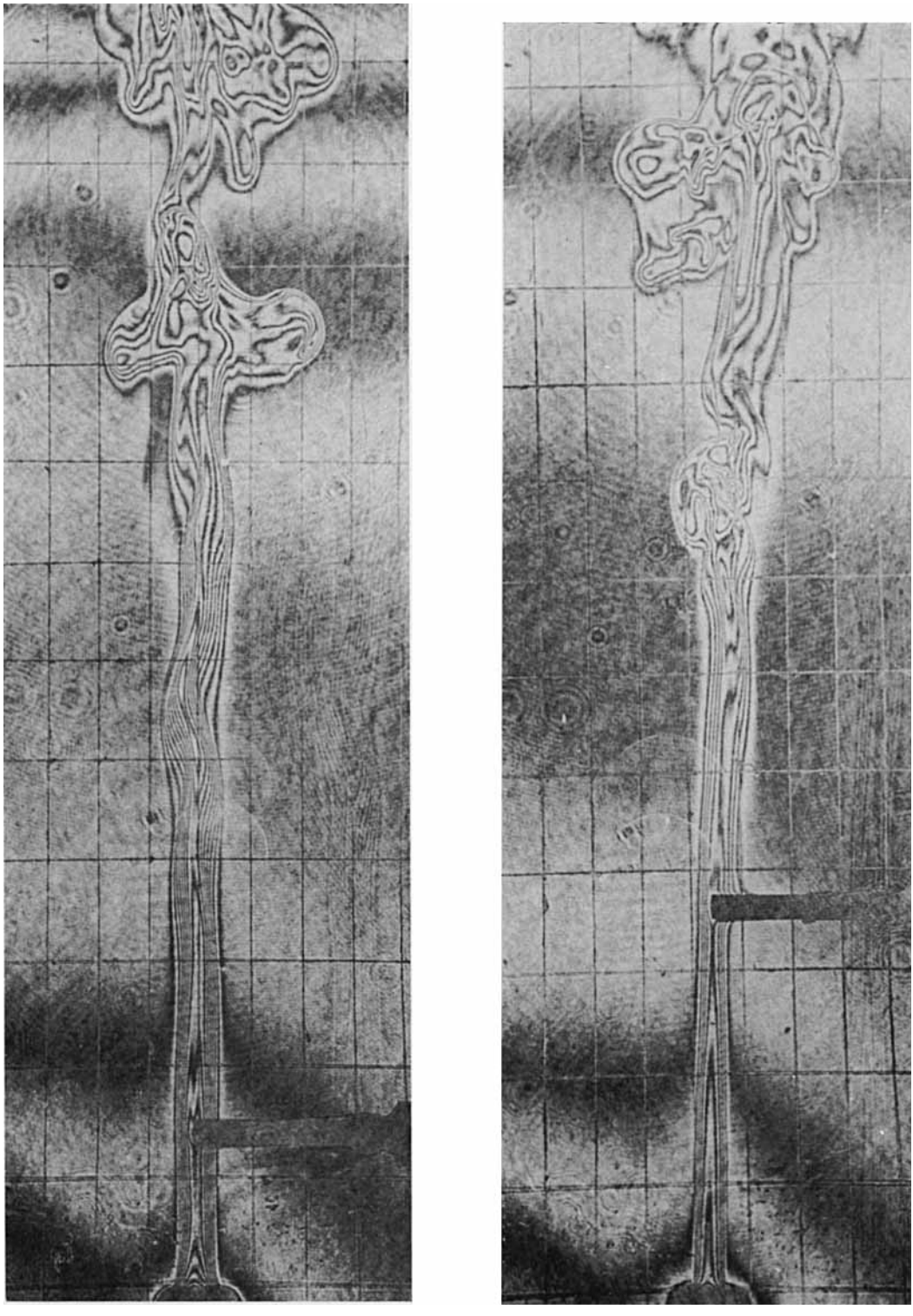

(*a*) (*b*)

FIGURE 13. Naturally occurring breakdown for (*a*) $Re_D = 250$ ($R = 54{\cdot}2$), $t_j = 107$ °F, $t_\infty = 81$ °F, $D = \frac{1}{4}$ in. and (*b*) $Re_D = 370$ ($R = 80$), $t_j = 101$ °F, $t_\infty = 81{\cdot}2$ °F, $D = \frac{1}{8}$ in.

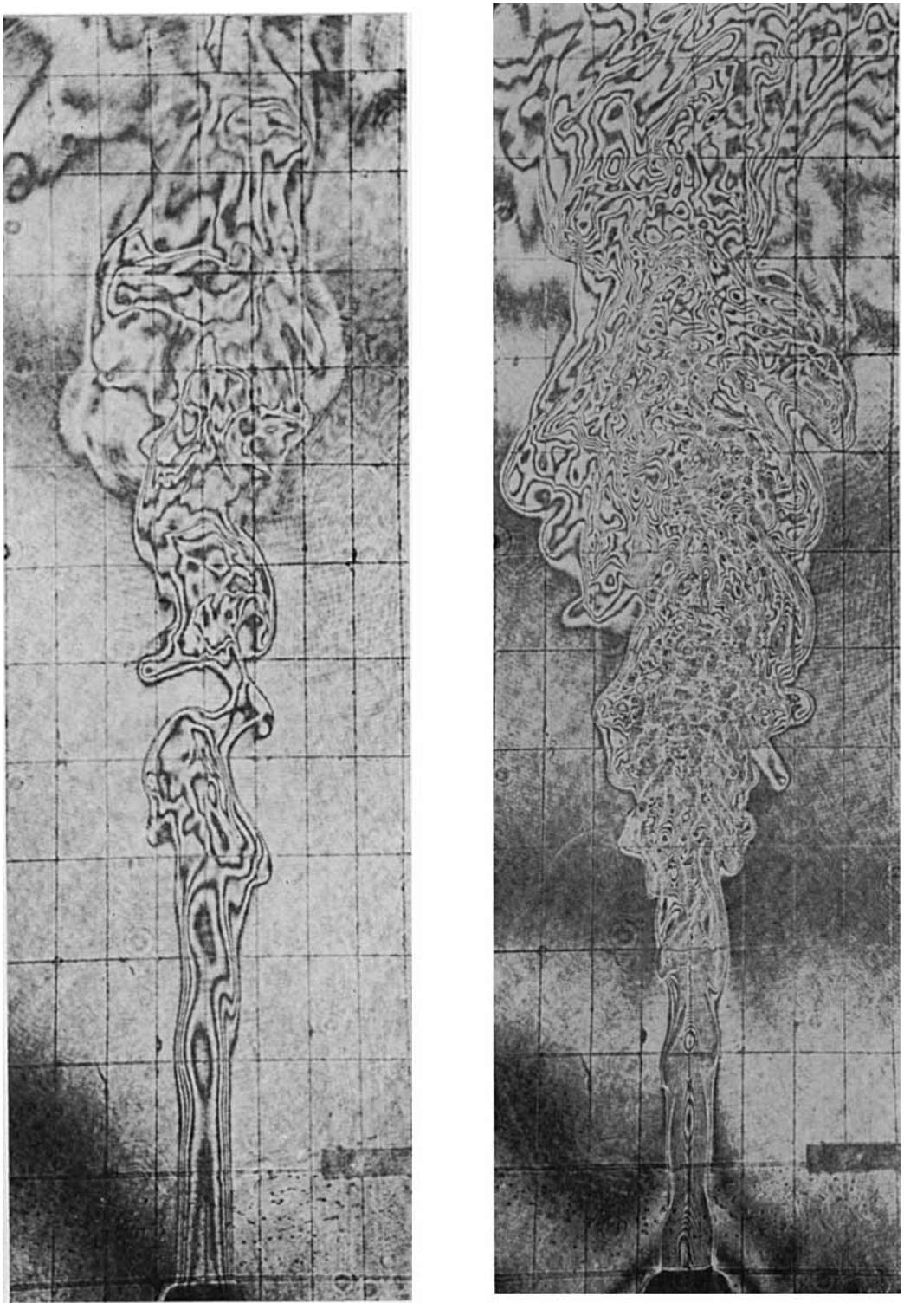

(*a*) (*b*)

FIGURE 14. Naturally occurring breakdown for (*a*) $Re_D = 537$ ($R = 117$), $t_j = 85$ °F and (*b*) $Re_D = 855$ ($R = 185$), $t_j = 116$ °F. $t_\infty = 82$ °F, $D = \frac{1}{4}$ in.

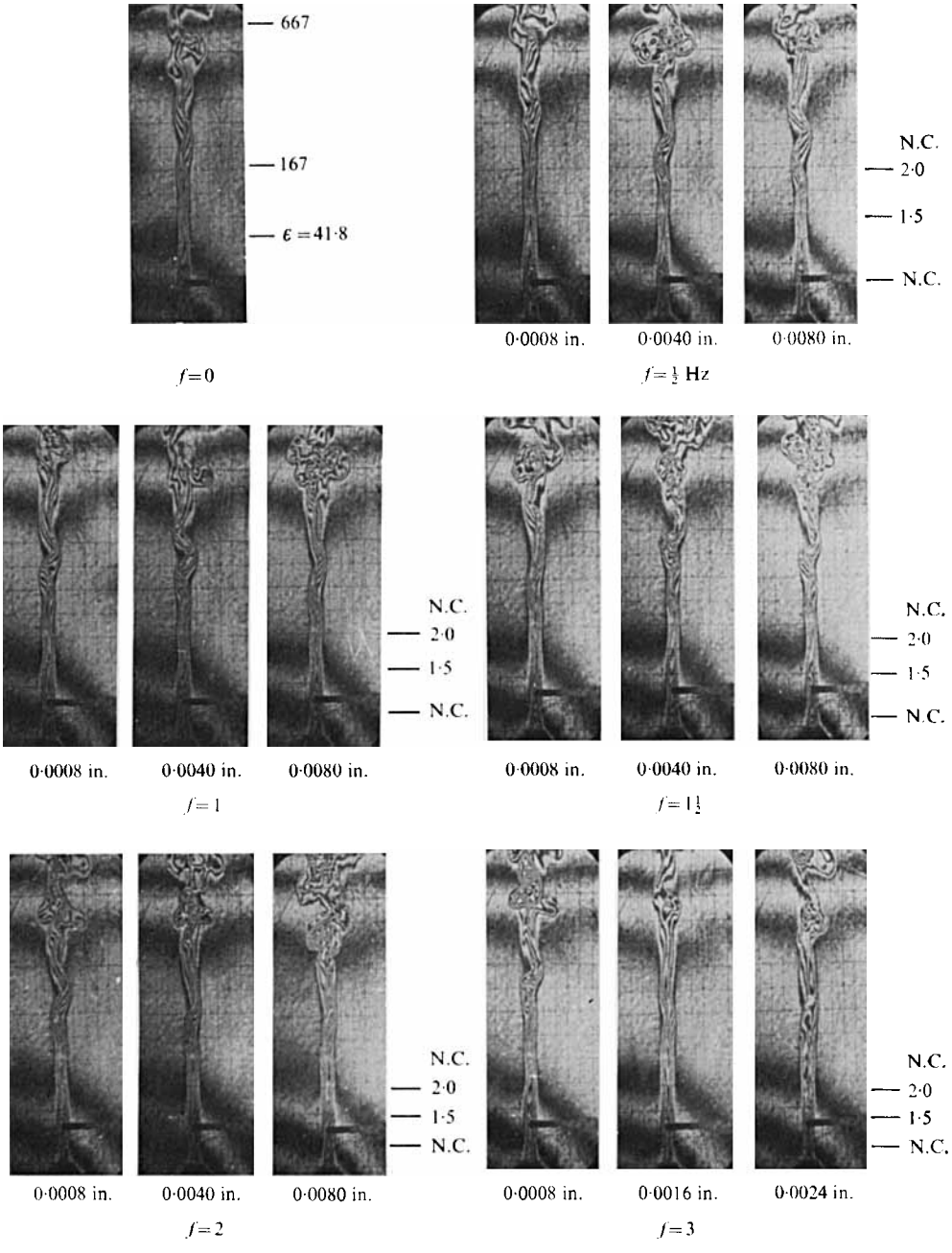

FIGURE 15. Response to artificially introduced disturbances for $Re_D = 138$ ($R = 30$), $t_j = 101\ °F$, $t_\infty = 82\ °F$, $D = \frac{1}{4}$ in.

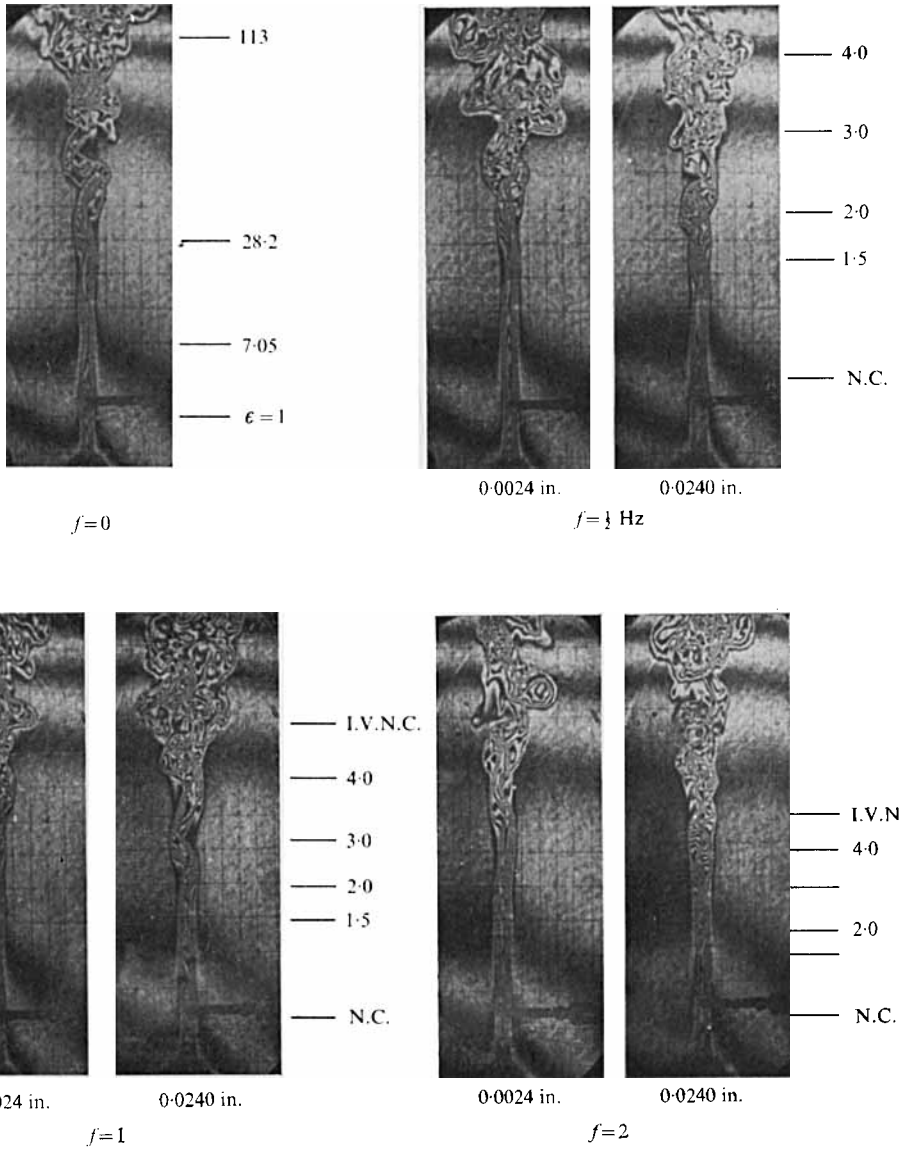

FIGURE 16. Response to artificially introduced disturbances for $Re_D = 250$ ($R = 54{\cdot}2$), $t_j = 107$ °F, $t_\infty = 81$ °F, $D = \frac{1}{4}$ in.

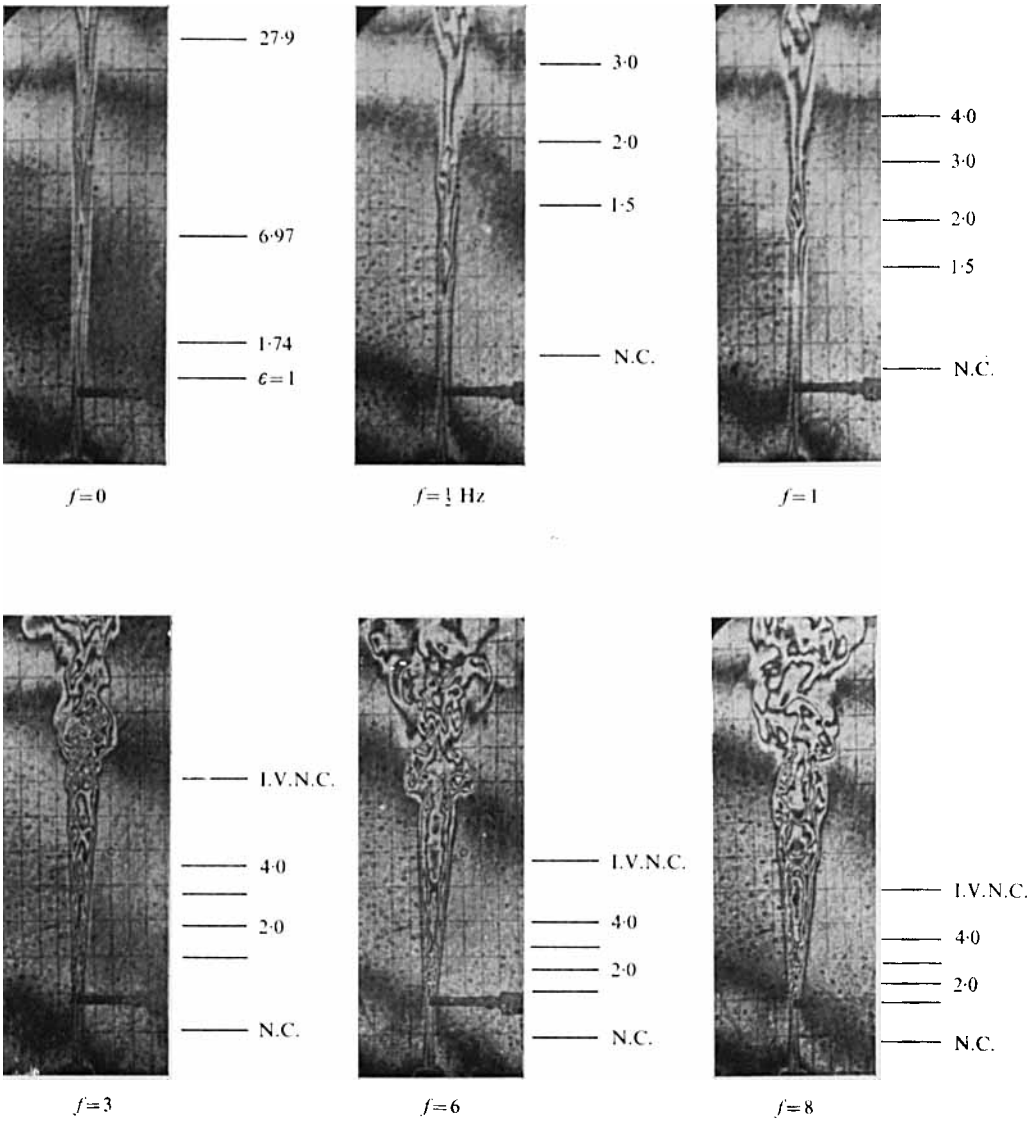

FIGURE 17. Response to artificially introduced disturbances for $Re_D = 316$ ($R = 68{\cdot}4$), $t_j = 106$ °F, $t_\infty = 85$ °F, $D = \frac{1}{8}$ in.

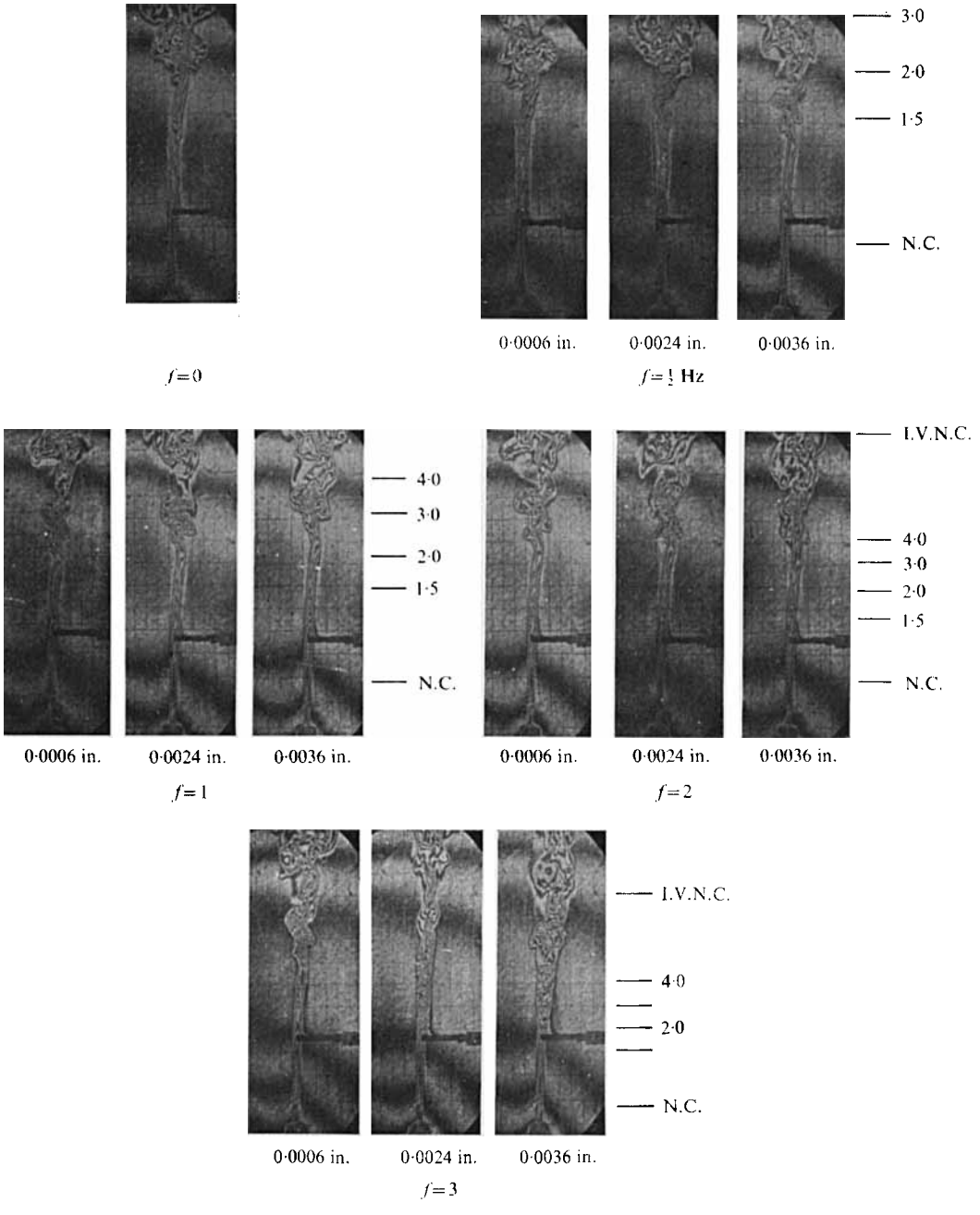

FIGURE 18. Response to artificially introduced disturbances for $Re_D = 370$ ($R = 80$), $t_j = 101$ °F, $t_\infty = 81{\cdot}2$ °F, $D = \frac{1}{8}$ in.

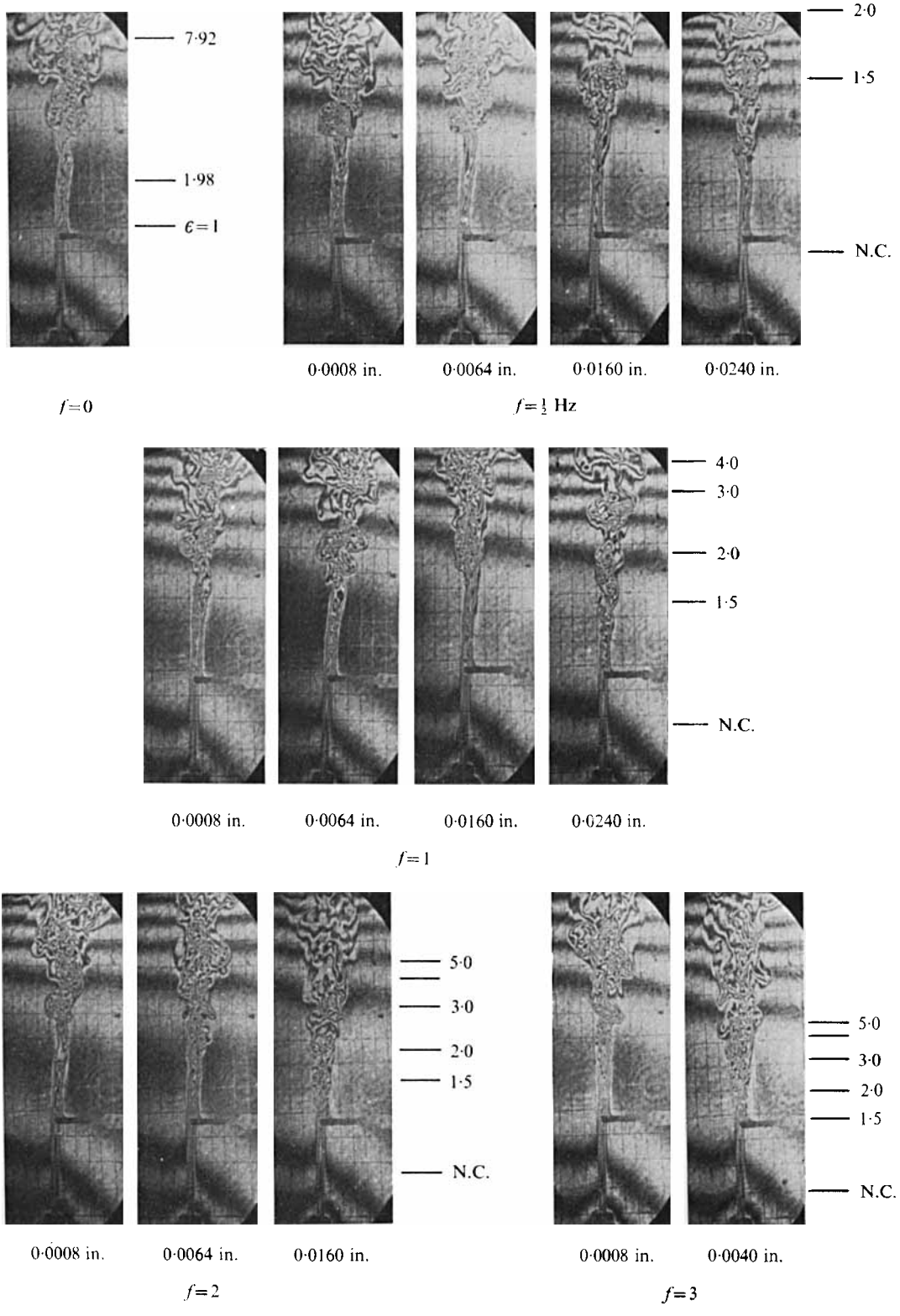

FIGURE 19. Response to artificially introduced disturbances for $Re_D = 481$ ($R = 104$), $t_j = 102$ °F, $t_\infty = 81$ °F, $D = \frac{1}{8}$ in.

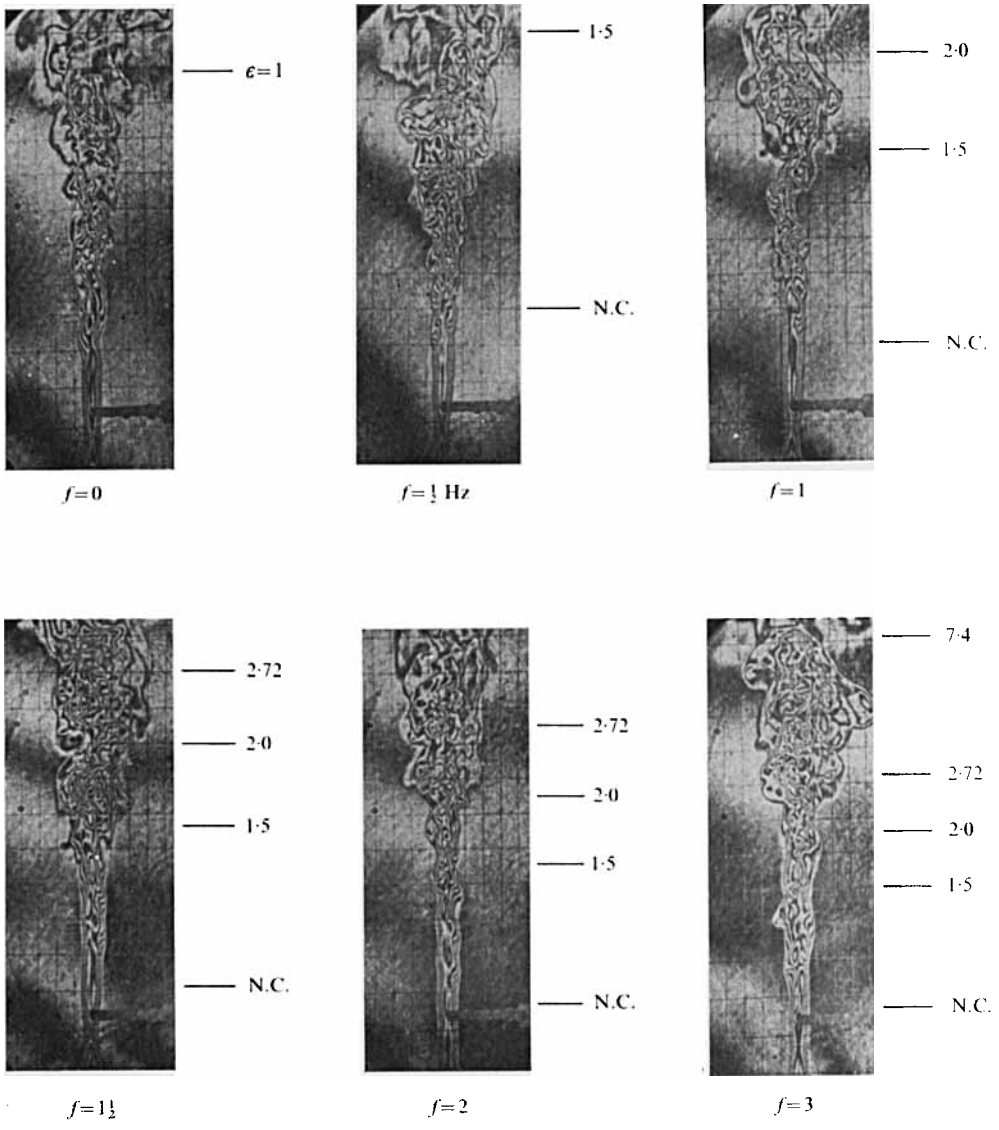

FIGURE 20. Response to artificially introduced disturbances for $Re_D = 537$ ($R = 117$), $t_j = 85\ ^\circ\mathrm{F}$, $t_\infty = 82\ ^\circ\mathrm{F}$, $D = \frac{1}{4}$ in.